

Probing SUSY effects in $K_S^0 \rightarrow \mu^+ \mu^-$

Veronika Chobanova,^(a) Giancarlo D'Ambrosio,^(b) Teppei Kitahara,^(c,d) Miriam Lucio Martínez,^(a) Diego Martínez Santos,^(a) Isabel Suárez Fernández^(a) and Kei Yamamoto^(e,f)

^(a)*Instituto Galego de Física de Altas Enerxías (IGFAE), Universidade de Santiago de Compostela, Rúa de Xoaquín Díaz de Rábago, s/n E-15782 Santiago de Compostela, Spain*

^(b)*INFN-Sezione di Napoli, Via Cintia, 80126 Napoli, Italia*

^(c)*Institute for Theoretical Particle Physics (TTP), Karlsruhe Institute of Technology, Engesserstraße 7, D-76128 Karlsruhe, Germany*

^(d)*Institute for Nuclear Physics (IKP), Karlsruhe Institute of Technology, Hermann-von-Helmholtz-Platz 1, D-76344 Eggenstein-Leopoldshafen, Germany*

^(e)*Department of Physics, Nagoya University, Nagoya 464-8602, Japan*

^(f)*Kobayashi-Maskawa Institute for the Origin of Particles and the Universe, Nagoya University, Nagoya 464-8602, Japan*

ABSTRACT: We explore supersymmetric contributions to the decay $K_S^0 \rightarrow \mu^+ \mu^-$, in light of current experimental data. The Standard Model (SM) predicts $\mathcal{B}(K_S^0 \rightarrow \mu^+ \mu^-) \approx 5 \times 10^{-12}$. We find that contributions arising from flavour violating Higgs penguins can enhance the branching fraction up to $\approx 35 \times 10^{-12}$ within different scenarios of the Minimal Supersymmetric Standard Model (MSSM), as well as suppress it down to $\approx 0.78 \times 10^{-12}$. Regions with fine-tuned parameters can bring the branching fraction up to the current experimental upper bound, 8×10^{-10} . The mass degeneracy of the heavy Higgs bosons in MSSM induces correlations between $\mathcal{B}(K_S^0 \rightarrow \mu^+ \mu^-)$ and $\mathcal{B}(K_L^0 \rightarrow \mu^+ \mu^-)$. Predictions for the CP asymmetry in $K^0 \rightarrow \mu^+ \mu^-$ decays in the context of MSSM are also given, and can be up to eight times bigger than in the SM.

KEYWORDS: Rare kaon decay, Supersymmetry, direct CP violation.

Contents

1	Introduction	1
2	Formalism	1
2.1	Definitions	1
2.2	Observables	2
2.3	$K^0 \rightarrow \mu^+ \mu^-$	3
2.4	$\varepsilon'_K / \varepsilon_K$	9
2.5	ε_K and ΔM_K	11
3	Parameter scan	13
4	Results	14
4.1	Effects from $\left(\delta_d^{LL(RR)}\right)_{12}$ separately	15
4.2	Floating LL and RR MIs simultaneously	22
4.3	Non degenerate Higgs masses	24
5	Conclusions	24
A	Wilson coefficients	25
A.1	$ \Delta S = 1$ gluino box contribution	25
A.2	$ \Delta S = 1$ chargino-mediated Z -penguin contribution	25
A.3	$ \Delta S = 1$ chromomagnetic dipole contribution	26
A.4	$ \Delta S = 2$ gluino box contribution	26
A.5	Sub-leading contributions to ε_K	26
B	Loop functions	27
B.1	$K^0 \rightarrow \mu^+ \mu^-$	27
B.2	$\varepsilon'_K / \varepsilon_K$	27
B.2.1	$ \Delta S = 1$ gluino box contributions	27
B.2.2	Chromomagnetic-dipole operator	28
B.3	ε_K	28
B.3.1	$ \Delta S = 2$ gluino box contributions	28
B.3.2	Wino and Higgsino contributions	29

1 Introduction

Leptonic decays of pseudoscalar mesons with down-type quarks are known to be very sensitive to the Higgs sector of the Minimal Supersymmetric Standard Model (MSSM), due to, among others, enhancement factors proportional to $(\tan^6 \beta / M_A^4)$.^{#1} This factor comes from the so-called non-holomorphic Yukawa terms at large $\tan \beta$ [1–6], which are triggered by the supersymmetric (SUSY) μ term, and hence the non-SUSY two-Higgs-doublet model cannot produce this enhancement [5]. The best known example is $B_s^0 \rightarrow \mu^+ \mu^-$ [1–15]. If Minimal Flavour Violation (MFV) is imposed, then $B_s^0 \rightarrow \mu^+ \mu^-$ is the dominant constraint in $P \rightarrow \mu^+ \mu^-$ decays. This is due to the stronger Yukawa coupling of the b -quark compared to the s -quark, and to the better experimental precision in $B_s^0 \rightarrow \mu^+ \mu^-$ compared to $B_d^0 \rightarrow \mu^+ \mu^-$. However, in the presence of new sources of flavour violation, the sensitivity of each mode depends on the flavour and CP structures of the corresponding terms. Hence, a priori, $B_s^0 \rightarrow \mu^+ \mu^-$, $B_d^0 \rightarrow \mu^+ \mu^-$, $K_S^0 \rightarrow \mu^+ \mu^-$, and $K_L^0 \rightarrow \mu^+ \mu^-$ are all separate constraints that carry complementary information in the general MSSM. The observables related to these decay modes are typically branching fractions and CP asymmetries. Even though the muon polarization could carry interesting information, it cannot be observed by current experiments.

In this paper, we focus on the MSSM effects in the $K_S^0 \rightarrow \mu^+ \mu^-$ decay. The Standard Model (SM) expectation is $(5.18 \pm 1.50_{\text{LD}} \pm 0.02_{\text{SD}}) \times 10^{-12}$ [16–18], where the first uncertainty comes from the long-distance (LD) contribution and the second one comes from the short-distance (SD) contribution. On the other hand, the current experimental upper bound is 8×10^{-10} at 90% C.L., using 3 fb^{-1} of LHCb data [19]. The LHCb upgrade could reach sensitivities at the level of about 1×10^{-11} or even below, approaching the SM prediction [20].

We predict the branching ratio $\mathcal{B}(K_S^0 \rightarrow \mu^+ \mu^-)$ under consideration of MSSM contributions and taking into account the relevant experimental constraints on the branching fractions $\mathcal{B}(K_L^0 \rightarrow \mu^+ \mu^-)$, $\mathcal{B}(B^+ \rightarrow \tau^+ \nu_\tau)$ and $\mathcal{B}(K^+ \rightarrow \mu^+ \nu_\mu)$, the CP violation parameters $\varepsilon'_K / \varepsilon_K$ and ε_K , the $K_L^0 - K_S^0$ mass difference, $\Delta M_K \equiv M_{K_L^0} - M_{K_S^0} > 0$, and the Wilson coefficient C_7 from $b \rightarrow s \gamma$. We use the Mass Insertion Approximation (MIA) [21], treating the mass insertion terms as phenomenological parameters at the SUSY scale. The details of the formalism are given in section 2. The subsets of the MSSM parameter space are studied in scans performed on Graphics Processing Units (GPU), as detailed in section 3. The results are shown in section 4 and conclusions are drawn in section 5.

2 Formalism

2.1 Definitions

In this paper, we follow the notations of ref. [22, 23]. We denote the right-handed down and up squarks as D and U . On the other hand, the two left-handed squarks have the same mass because of the $SU(2)_L$ doublet, and they are denoted as Q . The average of the Q , D , and U -squark masses squared are denoted by \tilde{m}_Q^2 , \tilde{m}_d^2 , \tilde{m}_u^2 , respectively.

^{#1}Note that this enhancement factor is not present in the up-type quark case.

The mass insertions (hereafter MIs) are defined as:

$$(\delta_d^{LL})_{ij} = \frac{[(\mathcal{M}_D^2)_{LL}]_{ij}}{\tilde{m}_Q^2} = \frac{(m_Q^2)_{ji}}{\tilde{m}_Q^2}, \quad (2.1)$$

$$(\delta_u^{LL})_{ij} = \frac{[(\mathcal{M}_U^2)_{LL}]_{ij}}{\tilde{m}_Q^2} = \frac{(Vm_Q^2 V^\dagger)_{ji}}{\tilde{m}_Q^2}, \quad (2.2)$$

$$(\delta_d^{RR})_{ij} = \frac{[(\mathcal{M}_D^2)_{RR}]_{ij}}{\tilde{m}_d^2} = \frac{(m_D^2)_{ij}}{\tilde{m}_d^2}, \quad (2.3)$$

where V is the Cabibbo–Kobayashi–Maskawa (CKM) matrix and $\mathcal{M}_{D,U}^2$ are the 6×6 squark mass matrices. Note that the indices ij are inverted for LL . Comparison with the SUSY Les Houches Accord 2 convention [24] is given in the appendix of ref. [22].

The running coupling constants α_1 , α_2 , and α_3 are defined as

$$\alpha_1 = \frac{g_1^2}{4\pi} = \frac{5}{3} \frac{g'^2}{4\pi}, \quad (2.4)$$

$$\alpha_2 = \frac{g_2^2}{4\pi} = \frac{g^2}{4\pi}, \quad (2.5)$$

$$\alpha_3 = \frac{g_3^2}{4\pi} = \frac{g_s^2}{4\pi}, \quad (2.6)$$

where g' , g , and g_s are the $U(1)_Y$, $SU(2)_L$, and $SU(3)_C$ group coupling constants, respectively. In the following, these couplings are evaluated at the μ^{SUSY} scale, where we define $\mu^{\text{SUSY}} = \sqrt{\tilde{m}_Q M_3}$.

2.2 Observables

As will be shown in the next subsections, the main MSSM contribution to $\mathcal{B}(K_S^0 \rightarrow \mu^+ \mu^-)$ is proportional to $\left[\left(\delta_d^{LL(RR)} \right)_{12} \mu \tan^3 \beta M_3 / M_A^2 \right]^2$. In order to constrain those parameters, the following observables are calculated in addition to $\mathcal{B}(K_S^0 \rightarrow \mu^+ \mu^-)$:

- Observables sensitive, among others, to the off-diagonal mass insertion terms $\left(\delta_d^{LL(RR)} \right)_{12}$: $\mathcal{B}(K_L^0 \rightarrow \mu^+ \mu^-)$, $\varepsilon'_K / \varepsilon_K$, ε_K , and ΔM_K .^{#2}
- Observables sensitive to $\tan \beta$ and the heavy Higgs mass: $\mathcal{B}(B^+ \rightarrow \tau^+ \nu_\tau)$, $\mathcal{B}(K^+ \rightarrow \mu^+ \nu_\mu)$, ΔC_7 .

The definitions of $\mathcal{B}(B^+ \rightarrow \tau^+ \nu_\tau)$, $\mathcal{B}(K^+ \rightarrow \mu^+ \nu_\mu)$, and C_7 are given in ref. [22] and the remaining observables are defined in the following subsections. The CKM matrix is fitted excluding measurements with potential sensitivity to MSSM contributions.

The constraints we impose on physics observables sensitive to the MSSM same parameters as $\mathcal{B}(K_S^0 \rightarrow \mu^+ \mu^-)$ are listed in table 1, where the EXP/SM represents the measured value over the SM prediction with their uncertainties. Due to the poor theoretical knowledge of ΔM_K , we assign a 100% theoretical uncertainty; thus, the constraint imposed on

^{#2} The contributions to $\mathcal{B}(K \rightarrow \pi \nu \bar{\nu})$ are controlled by an additional free parameter, the slepton mass, and $\mathcal{O}(1)$ effects are possible in this scenario [25].

Observable	Constraint
$\mathcal{B}(K_S^0 \rightarrow \mu^+ \mu^-)^{\text{EXP/SM}}$	unconstrained
$\mathcal{B}(K_L^0 \rightarrow \mu^+ \mu^-)^{\text{EXP/SM}}$	1.00 ± 0.12 (+) [18, 33, 34]
	0.84 ± 0.16 (-) [18, 33, 34]
$\Delta M_K^{\text{EXP/SM}}$	1 ± 1
$\varepsilon_K^{\text{EXP/SM}}$	1.05 ± 0.10 [34–36]
$\Delta(\varepsilon'_K/\varepsilon_K)^{\text{EXP-SM}}$	$[15.5 \pm 2.3(\text{EXP}) \pm 5.07(\text{TH})] \times 10^{-4}$ [34, 37]
$\mathcal{B}(B^+ \rightarrow \tau^+ \nu_\tau)^{\text{EXP/SM}}$	0.91 ± 0.22 [34]
$\mathcal{B}(K^+ \rightarrow \mu^+ \nu_\mu)^{\text{EXP/SM}}$	1.0004 ± 0.0095 [34]
ΔC_7	-0.02 ± 0.02 [38]
$\tan \beta: M_A$ plane	ATLAS limits for hMSSM scenario [39]
LSP	Lightest neutralino
B_G	$1 \pm 3(\text{TH})$ [40, 41]

Table 1. Physics observables constraints imposed in this study. The two different constraints on $\mathcal{B}(K_L^0 \rightarrow \mu^+ \mu^-)^{\text{EXP/SM}}$ arise from an unknown sign of $A_{L\gamma\gamma}^\mu$ in eq. (2.16) (see refs. [18, 33]).

this observable penalizes only $\mathcal{O}(1)$ effects. It is not counted as a degree of freedom in the χ^2 tests, so that the ΔM_K constraint can only make the bounds tighter, but never looser. Remaining constraints can in principle be satisfied by adjusting the other parameters of the model. In particular, B physics constraints not included in our list can be satisfied by parameters unspecified in our scan, for example by setting $\delta_{13} \approx \delta_{23} \approx 0$ and small A_t . The relation of eq. (2.2) may induce non-zero up-type MIs in the B sector and hence modify $B_{s(d)}^0 \rightarrow \mu^+ \mu^-$, however, we checked that these effects can be safely neglected in the scenarios we studied. The large SUSY masses in our scan are typically beyond the reach of LHC.

The lattice values for $(\varepsilon'_K/\varepsilon_K)^{\text{SM}}$ used are from refs. [26–29], although the conclusions of our study remain largely unchanged if we use the χ_{PT} value from refs. [30–32] instead. The values of $\varepsilon_K^{\text{EXP/SM}}$ and $\Delta(\varepsilon'_K/\varepsilon_K)^{\text{EXP-SM}}$ are discussed in more detail in the following subsections.

2.3 $K^0 \rightarrow \mu^+ \mu^-$

The $|\Delta S| = 1$ effective Hamiltonian relevant for the $K^0 \rightarrow \ell \bar{\ell}$ transition at the Z boson mass scale is

$$\mathcal{H}_{\text{eff}} = -C_A Q_A - \tilde{C}_A \tilde{Q}_A - C_S Q_S - \tilde{C}_S \tilde{Q}_S - C_P Q_P - \tilde{C}_P \tilde{Q}_P + \text{H.c.}, \quad (2.7)$$

where C_A , C_S and C_P are the axial, scalar and pseudoscalar Wilson coefficients. The right-handed and left-handed axial (\tilde{Q}_A , Q_A), scalar (Q_S , \tilde{Q}_S) and pseudoscalar (Q_P , \tilde{Q}_P)

operators are given by:

$$\begin{aligned}
Q_A &= (\bar{s}\gamma^\mu P_L d)(\bar{\ell}\gamma_\mu\gamma_5\ell), & \tilde{Q}_A &= (\bar{s}\gamma^\mu P_R d)(\bar{\ell}\gamma_\mu\gamma_5\ell), \\
Q_S &= m_s(\bar{s}P_R d)(\bar{\ell}\ell), & \tilde{Q}_S &= m_s(\bar{s}P_L d)(\bar{\ell}\ell), \\
Q_P &= m_s(\bar{s}P_R d)(\bar{\ell}\gamma_5\ell), & \tilde{Q}_P &= m_s(\bar{s}P_L d)(\bar{\ell}\gamma_5\ell),
\end{aligned} \tag{2.8}$$

where $P_{L,R}$ are the left and right-handed projection operators. For $\mathcal{B}(K_{S,L}^0 \rightarrow \mu^+\mu^-)$ ^{#3}, there are two contributions from S-wave ($A_{S,L}$) and P-wave transitions ($B_{S,L}$), resulting in: ^{#4}

$$\mathcal{B}(K_{S,L}^0 \rightarrow \mu^+\mu^-) = \tau_{S,L}\Gamma(K_{S,L}^0 \rightarrow \mu^+\mu^-) = \tau_{S,L}\frac{f_K^2 M_K^3 \beta_\mu}{16\pi} (|A_{S,L}|^2 + \beta_\mu^2 |B_{S,L}|^2), \tag{2.9}$$

with

$$A_S = \frac{m_s M_K}{m_s + m_d} \text{Im}(C_P - \tilde{C}_P) + \frac{2m_\mu}{M_K} \text{Im}(C_A - \tilde{C}_A), \tag{2.10}$$

$$B_S = \frac{2G_F^2 M_W^2 m_\mu}{\pi^2 M_K} B_{S\gamma\gamma}^\mu - \frac{m_s M_K}{m_s + m_d} \text{Re}(C_S - \tilde{C}_S), \tag{2.11}$$

and

$$A_L = \frac{2G_F^2 M_W^2 m_\mu}{\pi^2 M_K} A_{L\gamma\gamma}^\mu - \frac{m_s M_K}{m_s + m_d} \text{Re}(C_P - \tilde{C}_P) - \frac{2m_\mu}{M_K} \text{Re}(C_A - \tilde{C}_A), \tag{2.12}$$

$$B_L = \frac{m_s M_K}{m_s + m_d} \text{Im}(C_S - \tilde{C}_S), \tag{2.13}$$

where

$$\beta_\mu = \sqrt{1 - \frac{4m_\mu^2}{M_K^2}}. \tag{2.14}$$

Here, the long-distance contributions are [16–18, 42]:^{#5}

$$\frac{2G_F^2 M_W^2 m_\mu}{\pi^2 M_K} B_{S\gamma\gamma}^\mu = (-2.65 + 1.14i) \times 10^{-11} (\text{GeV})^{-2}, \tag{2.15}$$

$$\frac{2G_F^2 M_W^2 m_\mu}{\pi^2 M_K} A_{L\gamma\gamma}^\mu = \pm(0.54 - 3.96i) \times 10^{-11} (\text{GeV})^{-2}, \tag{2.16}$$

and $\tau_{S,L}$ are the $K_{S,L}^0$ lifetimes. Here, $f_K = (155.9 \pm 0.4)$ MeV [34]. Note that there is a theoretically and experimentally unknown sign in $A_{L\gamma\gamma}^\mu$, which is determined by higher chiral orders than $\mathcal{O}(p^4)$ contributions [46, 47], and they provide two different constraints on $\mathcal{B}(K_L^0 \rightarrow \mu^+\mu^-)^{\text{EXP/SM}}$ in table 1. This sign can be determined by a precise measurement of the interference between $K_L^0 \rightarrow \mu^+\mu^-$ and $K_S^0 \rightarrow \mu^+\mu^-$ [18]. In addition, in the MSSM,

^{#3} The electron modes are suppressed by m_e^2/m_μ^2 , and we do not consider them in this paper.

^{#4} Our result agrees with refs. [42–45]. However, it disagrees with notable literature [6, 22] after discarding the long-distance contributions. We found that C_{10}^{SM} should be $-C_{10}^{\text{SM}}$ in eq. (3.45) of ref. [22], and $(C_P - C'_P)$ should be $(C'_P - C_P)$ in eq. (2.4) of ref. [6].

^{#5} Note that $B_{S\gamma\gamma}^\mu$ is denoted by $A_{S\gamma\gamma}^\mu$ in refs. [18, 42].

the correlation between $\mathcal{B}(K_S^0 \rightarrow \mu^+ \mu^-)$ and $\mathcal{B}(K_L^0 \rightarrow \mu^+ \mu^-)$ depends on the unknown sign of $A_{L\gamma\gamma}^\mu$. In the following, we derive some relations between the two branching fractions, for a better interpretation of the results of our scans. In the case in which new physics enters only in \tilde{C}_S and $\tilde{C}_P = \tilde{C}_S$ (pure left-handed MSSM scenario), the following relations between the branching fractions of K_S^0 and K_L^0 decaying into $\mu^+ \mu^-$ can be established:

$$\mathcal{B}(K_S^0 \rightarrow \mu^+ \mu^-) \propto \beta_\mu^2 |N_S^{\text{LD}}|^2 + (A_{S,\text{SM}}^{\text{SD}})^2 - 2M_K \left[A_{S,\text{SM}}^{\text{SD}} \text{Im}(\tilde{C}_S) - \beta_\mu^2 \text{Re}(N_S^{\text{LD}}) \text{Re}(\tilde{C}_S) \right] + M_K^2 \left\{ \left[\text{Im}(\tilde{C}_S) \right]^2 + \beta_\mu^2 \left[\text{Re}(\tilde{C}_S) \right]^2 \right\}, \quad (2.17)$$

$$\mathcal{B}(K_L^0 \rightarrow \mu^+ \mu^-) \propto |N_L^{\text{LD}}|^2 + (A_{L,\text{SM}}^{\text{SD}})^2 - 2M_K \text{Re}(\tilde{C}_S) \left[A_{L,\text{SM}}^{\text{SD}} - \text{Re}(N_L^{\text{LD}}) \right] + M_K^2 \left\{ \left[\text{Re}(\tilde{C}_S) \right]^2 + \beta_\mu^2 \left[\text{Im}(\tilde{C}_S) \right]^2 \right\} - 2A_{L,\text{SM}}^{\text{SD}} \text{Re}(N_L^{\text{LD}}), \quad (2.18)$$

with

$$A_{S,\text{SM}}^{\text{SD}} = \frac{2m_\mu}{M_K} \text{Im}(C_{A,\text{SM}}), \quad A_{L,\text{SM}}^{\text{SD}} = \frac{2m_\mu}{M_K} \text{Re}(C_{A,\text{SM}}), \quad (2.19)$$

and

$$N_S^{\text{LD}} = \frac{2G_F^2 M_W^2 m_\mu}{\pi^2 M_K} B_{S\gamma\gamma}^\mu, \quad N_L^{\text{LD}} = \frac{2G_F^2 M_W^2 m_\mu}{\pi^2 M_K} A_{L\gamma\gamma}^\mu, \quad (2.20)$$

where m_d terms are discarded for simplicity. The long-distance term $\text{Re}(N_L^{\text{LD}})$ holds the unknown sign from $A_{L\gamma\gamma}^\mu$, which changes the correlation significantly, as will be shown. On the other hand, if new physics produces only C_S and $C_P = -C_S$ (pure right-handed MSSM), the two branching fractions are

$$\mathcal{B}(K_S^0 \rightarrow \mu^+ \mu^-) \propto \beta_\mu^2 |N_S^{\text{LD}}|^2 + (A_{S,\text{SM}}^{\text{SD}})^2 - 2M_K \left[A_{S,\text{SM}}^{\text{SD}} \text{Im}(C_S) + \beta_\mu^2 \text{Re}(N_S^{\text{LD}}) \text{Re}(C_S) \right] + M_K^2 \left\{ \left[\text{Im}(C_S) \right]^2 + \beta_\mu^2 \left[\text{Re}(C_S) \right]^2 \right\}, \quad (2.21)$$

$$\mathcal{B}(K_L^0 \rightarrow \mu^+ \mu^-) \propto |N_L^{\text{LD}}|^2 + (A_{L,\text{SM}}^{\text{SD}})^2 - 2M_K \text{Re}(C_S) \left[A_{L,\text{SM}}^{\text{SD}} - \text{Re}(N_L^{\text{LD}}) \right] + M_K^2 \left\{ \left[\text{Re}(C_S) \right]^2 + \beta_\mu^2 \left[\text{Im}(C_S) \right]^2 \right\} - 2A_{L,\text{SM}}^{\text{SD}} \text{Re}(N_L^{\text{LD}}). \quad (2.22)$$

It is shown that $\mathcal{B}(K_L^0 \rightarrow \mu^+ \mu^-)$ is the same as the pure left-handed one by a replacement of $C_S \rightarrow \tilde{C}_S$, while $\mathcal{B}(K_S^0 \rightarrow \mu^+ \mu^-)$ is not; the final terms of the first line have opposite sign. Hence, the relations between the two branching fractions are different for left-handed and right-handed new physics scenarios.

For those cases, the experimental measurement of $\mathcal{B}(K_L^0 \rightarrow \mu^+ \mu^-)$ [34],

$$\mathcal{B}(K_L^0 \rightarrow \mu^+ \mu^-)^{\text{EXP}} = (6.84 \pm 0.11) \times 10^{-9}, \quad (2.23)$$

imposes an upper bound on $\mathcal{B}(K_S^0 \rightarrow \mu^+ \mu^-)$. This bound can be alleviated if $|C_S| \neq |C_P|$ or if new physics is present simultaneously in the left-handed and right-handed Wilson coefficients.

Experimentally, one can also access an *effective* branching ratio of $K_S^0 \rightarrow \mu^+\mu^-$ [18] which includes an interference contribution with $K_L^0 \rightarrow \mu^+\mu^-$ in the neutral kaon sample. We obtain

$$\mathcal{B}(K_S^0 \rightarrow \mu^+\mu^-)_{\text{eff}} = \tau_S \left(\int_{t_{\min}}^{t_{\max}} dt e^{-\Gamma_S t} \varepsilon(t) \right)^{-1} \left[\int_{t_{\min}}^{t_{\max}} dt \left\{ \Gamma(K_S^0 \rightarrow \mu^+\mu^-) e^{-\Gamma_S t} + \frac{D f_K^2 M_K^3 \beta_\mu}{8\pi} \text{Re} [i (A_S A_L - \beta_\mu^2 B_S^* B_L) e^{-i\Delta M_K t}] e^{-\frac{\Gamma_S + \Gamma_L}{2} t} \right\} \varepsilon(t) \right], \quad (2.24)$$

where the dilution factor D is a measure of the initial ($t = 0$) $K^0 - \bar{K}^0$ asymmetry,

$$D = \frac{K^0 - \bar{K}^0}{K^0 + \bar{K}^0}, \quad (2.25)$$

$\varepsilon(t)$ is the decay-time acceptance of the detector. The second line of eq. (2.24) corresponds to an interference effect between K_L^0 and K_S^0 , and for $D = 0$, $\mathcal{B}(K_S^0 \rightarrow \mu^+\mu^-)_{\text{eff}}$ corresponds to $\mathcal{B}(K_S^0 \rightarrow \mu^+\mu^-)$. The current experimental bound [19],

$$\mathcal{B}(K_S^0 \rightarrow \mu^+\mu^-)^{\text{EXP}} < 8 \times 10^{-10} \text{ [90\% C.L.]}, \quad (2.26)$$

uses untagged K^0 and \bar{K}^0 mesons produced in almost equal amounts, and hence $D = 0$ is assumed. A pure $K_L^0 \rightarrow \mu^+\mu^-$ background can be subtracted by a combination of simultaneous measurement of $K_S^0 \rightarrow \pi^+\pi^-$ events and knowledge of the observed value of $\mathcal{B}(K_L^0 \rightarrow \mu^+\mu^-)$ in eq. (2.23) [18]. The decay-time acceptance of the LHCb detector is parametrized by $\varepsilon(t) = \exp(-\beta t)$ with $\beta \simeq 86 \text{ ns}^{-1}$, and the range of the detector for selecting $K^0 \rightarrow \mu^+\mu^-$ is $t_{\min} = 8.95 \text{ ps} = 0.1\tau_S$ and $t_{\max} = 130 \text{ ps} = 1.45\tau_S$.

Given the potential measurement of an effective branching ratio by different dilution factors $D > 0$ and $D' < 0$ using K^- tagging and K^+ tagging, respectively, the direct CP asymmetry can be measured using the difference $\mathcal{B}(K_S^0 \rightarrow \mu^+\mu^-)_{\text{eff}}(D) - \mathcal{B}(K_S^0 \rightarrow \mu^+\mu^-)_{\text{eff}}(D')$, which is a theoretically clean quantity that emerges from a genuine direct CP violation. Therefore, we define the following direct CP asymmetry in $K_S^0 \rightarrow \mu^+\mu^-$:

$$A_{CP}(K_S^0 \rightarrow \mu^+\mu^-)_{D,D'} = \frac{\mathcal{B}(K_S^0 \rightarrow \mu^+\mu^-)_{\text{eff}}(D) - \mathcal{B}(K_S^0 \rightarrow \mu^+\mu^-)_{\text{eff}}(D')}{\mathcal{B}(K_S^0 \rightarrow \mu^+\mu^-)_{\text{eff}}(D) + \mathcal{B}(K_S^0 \rightarrow \mu^+\mu^-)_{\text{eff}}(D')}. \quad (2.27)$$

We discarded the indirect CP -violating contributions because they are numerically negligible compared to the CP -conserving and the direct CP -violating contributions [18].

Within the SM, the Wilson coefficients are,

$$C_{A,\text{SM}} = -\frac{[\alpha_2(M_Z)]^2}{2M_W^2} (V_{ts}^* V_{td} Y_t + V_{cs}^* V_{cd} Y_c), \quad (2.28)$$

$$\tilde{C}_{A,\text{SM}} = C_{S,\text{SM}} = \tilde{C}_{S,\text{SM}} = C_{P,\text{SM}} = \tilde{C}_{P,\text{SM}} \simeq 0, \quad (2.29)$$

where $Y_t = 0.950 \pm 0.049$ and $Y_c = (2.95 \pm 0.46) \times 10^{-4}$ [48]. Using the CKM matrix tailored for probing the MSSM contributions, we obtain the SM prediction of A_{CP} ,

$$A_{CP}(K_S^0 \rightarrow \mu^+\mu^-)_{D,D'}^{\text{SM}} = \begin{cases} -\frac{3.71(D-D')}{(10.53 \pm 3.01) - 3.71(D+D')}, & (+) \\ \frac{3.98(D-D')}{(10.53 \pm 3.01) + 3.98(D+D')}, & (-) \end{cases} \quad (2.30)$$

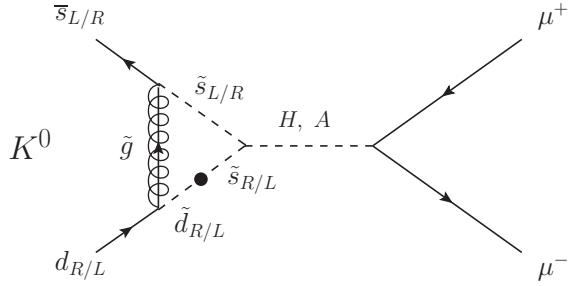


Figure 1. Feynman diagram of the leading (pseudo-)scalar MSSM contributions to $K_S^0 \rightarrow \mu^+ \mu^-$ and $K_L^0 \rightarrow \mu^+ \mu^-$, which include a gluino and a heavy Higgs boson. The black dot is the corresponding mass insertion term.

where (+) and (-) correspond to the unknown sign of $A_{L\gamma\gamma}^\mu$ in eq. (2.16). The uncertainty is totally dominated by $B_{S\gamma\gamma}^\mu$ [18] and it will be sharpened by the dispersive treatment of $K_S^0 \rightarrow \gamma^{(*)}\gamma^{(*)}$ [49]. If one considers the case of $D' = -D$ achieved by the accompanying opposite-charged-kaon tagging, the SM prediction of A_{CP} is simplified:

$$A_{CP}(K_S^0 \rightarrow \mu^+ \mu^-)_{D,-D}^{\text{SM}} = \begin{cases} (-0.704_{-0.281}^{+0.156}) \times D, (+) \\ (+0.756_{-0.168}^{+0.302}) \times D, (-) \end{cases} \quad (2.31)$$

In the MSSM, the leading contribution to C_A , induced by terms of second order in the expansion of the squark mass matrix of the chargino Z -penguin, is [6, 50],

$$C_A = -\frac{(\alpha_2)^2}{16M_W^2} \frac{[(\mathcal{M}_U^2)_{LR}]_{23}^* [(\mathcal{M}_U^2)_{LR}]_{13}}{M_2^4} l(x_2^Q, x_2^u), \quad (2.32)$$

$$\tilde{C}_A = 0, \quad (2.33)$$

where $x_2^Q = \tilde{m}_Q^2/M_2^2$ and $x_2^u = \tilde{m}_u^2/M_2^2$. The loop function $l(x, y)$ [50] is defined in appendix B.1. Here, contributions from the Wino-Higgsino mixing are omitted. Setting $\tilde{m}_Q^2 = \tilde{m}_u^2$ gives the MIA result of refs. [40, 51].

The leading MSSM contributions to $C_{S(P)}$ and $\tilde{C}_{S(P)}$ in $K_S^0 \rightarrow \mu^+ \mu^-$ and $K_L^0 \rightarrow \mu^+ \mu^-$

are shown in figure 1. For C_S and \tilde{C}_S , we obtain

$$\begin{aligned}
C_S = & -\frac{2}{3} \frac{\alpha_s \alpha_2 m_\mu}{M_W^2} \frac{\mu M_3}{M_A^2 \tilde{m}_d^2} (\delta_d^{RR})_{12} \frac{\tan^3 \beta}{(1 + \epsilon_g \tan \beta)^2 (1 + \epsilon_\ell \tan \beta)} G(x_d^3, x_d^Q) \\
& -\frac{2}{3} \frac{\alpha_s \alpha_2 m_\mu}{M_W^2} \frac{m_b}{m_s} \frac{\mu M_3 \tilde{m}_Q^2}{M_A^2 \tilde{m}_d^4} (\delta_d^{RR})_{13} (\delta_d^{LL})_{32} \\
& \times \frac{\tan^3 \beta}{(1 + \epsilon_g \tan \beta)[1 + (\epsilon_g + \epsilon_Y y_t^2) \tan \beta](1 + \epsilon_\ell \tan \beta)} H(x_d^3, x_d^Q), \tag{2.34}
\end{aligned}$$

$$\begin{aligned}
\tilde{C}_S = & -\frac{2}{3} \frac{\alpha_s \alpha_2 m_\mu}{M_W^2} \frac{\mu M_3}{M_A^2 \tilde{m}_Q^2} (\delta_d^{LL})_{12} \frac{\tan^3 \beta}{(1 + \epsilon_g \tan \beta)^2 (1 + \epsilon_\ell \tan \beta)} G(x_Q^3, x_Q^d) \\
& -\frac{2}{3} \frac{\alpha_s \alpha_2 m_\mu}{M_W^2} \frac{m_b}{m_s} \frac{\mu M_3 \tilde{m}_d^2}{M_A^2 \tilde{m}_Q^4} (\delta_d^{LL})_{13} (\delta_d^{RR})_{32} \\
& \times \frac{\tan^3 \beta}{(1 + \epsilon_g \tan \beta)[1 + (\epsilon_g + \epsilon_Y y_t^2) \tan \beta](1 + \epsilon_\ell \tan \beta)} H(x_Q^3, x_Q^d) \\
& + \frac{(\alpha_2)^2 m_\mu m_t^2}{8M_W^4} \frac{\mu A_t}{M_A^2 \tilde{m}_Q^2} V_{ts}^* V_{td} \frac{\tan^3 \beta [1 + (\epsilon_g + \epsilon_Y y_t^2) \tan \beta]^2}{(1 + \epsilon_g \tan \beta)^4 (1 + \epsilon_\ell \tan \beta)} F(x_Q^\mu, x_Q^u) \\
& + \frac{(\alpha_2)^2 m_\mu}{4M_W^2} \frac{\mu M_2}{M_A^2 \tilde{m}_Q^2} (\delta_u^{LL})_{12} \frac{\tan^3 \beta}{(1 + \epsilon_g \tan \beta)^2 (1 + \epsilon_\ell \tan \beta)} G(x_Q^2, x_Q^\mu), \tag{2.35}
\end{aligned}$$

with

$$\epsilon_g = \frac{2\alpha_s}{3\pi} \frac{\mu M_3}{\tilde{m}_Q^2} F(x_Q^3, x_Q^d), \tag{2.36}$$

$$\epsilon_Y = \frac{1}{16\pi} \frac{\mu A_t}{\tilde{m}_Q^2} F(x_Q^\mu, x_Q^u), \tag{2.37}$$

$$\epsilon_\ell \simeq -\frac{3\alpha_2}{16\pi}, \tag{2.38}$$

where $x_d^3 = M_3^2/\tilde{m}_d^2$, $x_d^Q = \tilde{m}_Q^2/\tilde{m}_d^2$, $x_Q^3 = M_3^2/\tilde{m}_Q^2$, $x_Q^d = \tilde{m}_d^2/\tilde{m}_Q^2$, $x_Q^\mu = \mu^2/\tilde{m}_Q^2$, $x_Q^u = \tilde{m}_u^2/\tilde{m}_Q^2$, $x_Q^2 = M_2^2/\tilde{m}_Q^2$, and $x_Q^\mu = \mu^2/\tilde{m}_Q^2$. The loop functions $F(x, y)$, $G(x, y)$, and $H(x, y)$ are defined in appendix B.1. These results are consistent with ref. [22] in the universal squark mass limit after changing the flavor and its chirality for B_s^0 decay. Here, we used the following approximation

$$\alpha \simeq \beta - \frac{\pi}{2}, \quad M_H \simeq M_A, \tag{2.39}$$

where α is an angle of the orthogonal rotation matrix for the CP -even Higgs mass, and M_H (M_A) is a CP -even (odd) heavy Higgs mass. On the other hand, the contributions to C_P and \tilde{C}_P are

$$C_P = -C_S, \quad \tilde{C}_P = \tilde{C}_S. \tag{2.40}$$

Note that the Wilson coefficients in the MSSM are given at the μ^{SUSY} scale, and there is no QCD correction from the renormalization-group (RG) evolution at the leading order.

2.4 $\varepsilon'_K/\varepsilon_K$

New physics models affecting $\varepsilon'_K/\varepsilon_K$ have recently attracted some attention since lattice results from the RBC and UKQCD collaborations [26–29] have been reported 2–3 σ below [37, 52] the experimental world average of $\text{Re}(\varepsilon'_K/\varepsilon_K)$ [34]. This is consistent with the recent calculations in the large- N_c analyses [53, 54]. Although the lattice simulation [29] includes final-state interactions partially along the line of ref. [55], final-state interactions have to be still fully included in the calculations in light of a discrepancy of a strong phase shift δ_0 [56–58]. Conversely combining large- N_c methods with chiral loop corrections can bring the value of $\varepsilon'_K/\varepsilon_K$ in agreement with the experiment [30–32].

In this paper, we used the hadronic matrix elements obtained by lattice simulations. For the χ^2 test, we use the following constraint,

$$\Delta \left(\frac{\varepsilon'_K}{\varepsilon_K} \right)^{\text{EXP-SM}} \equiv \text{Re} \left(\frac{\varepsilon'_K}{\varepsilon_K} \right)^{\text{EXP}} - \left(\frac{\varepsilon'_K}{\varepsilon_K} \right)^{\text{SM}} = [15.5 \pm 2.3(\text{EXP}) \pm 5.07(\text{TH})] \times 10^{-4}, \quad (2.41)$$

with

$$\left(\frac{\varepsilon'_K}{\varepsilon_K} \right)^{\text{SM}} \rightarrow \left(\frac{\varepsilon'_K}{\varepsilon_K} \right)^{\text{SM}} + \left(\frac{\varepsilon'_K}{\varepsilon_K} \right)^{\text{SUSY}}, \quad (2.42)$$

where the SM prediction at the next-to-leading order in ref. [37] is used. The experimental value of ε_K is used in the calculation of the ratio. The SUSY contributions to ε_K are given in the next subsection.

Within the MSSM, the SUSY contributions to $\varepsilon'_K/\varepsilon_K$ are dominated by gluino box, chargino-mediated Z -penguin, and chromomagnetic dipole contributions. The first two contributions are represented by the same $|\Delta S| = 1$ four-quark effective Hamiltonian at the μ^{SUSY} scale, which is:

$$\mathcal{H}_{\text{eff}} = \frac{G_F}{\sqrt{2}} \sum_q \sum_{i=1}^4 \left[C_i^q Q_i^q + \tilde{C}_i^q \tilde{Q}_i^q \right] + \text{H.c.}, \quad (2.43)$$

with

$$\begin{aligned} Q_1^q &= (\bar{s}d)_{V-A} (\bar{q}q)_{V+A}, & \tilde{Q}_1^q &= (\bar{s}d)_{V+A} (\bar{q}q)_{V-A}, \\ Q_2^q &= (\bar{s}_\alpha d_\beta)_{V-A} (\bar{q}_\beta q_\alpha)_{V+A}, & \tilde{Q}_2^q &= (\bar{s}_\alpha d_\beta)_{V+A} (\bar{q}_\beta q_\alpha)_{V-A}, \\ Q_3^q &= (\bar{s}d)_{V-A} (\bar{q}q)_{V-A}, & \tilde{Q}_3^q &= (\bar{s}d)_{V+A} (\bar{q}q)_{V+A}, \\ Q_4^q &= (\bar{s}_\alpha d_\beta)_{V-A} (\bar{q}_\beta q_\alpha)_{V-A}, & \tilde{Q}_4^q &= (\bar{s}_\alpha d_\beta)_{V+A} (\bar{q}_\beta q_\alpha)_{V+A}, \end{aligned} \quad (2.44)$$

where $(V \mp A)$ refers to $\gamma_\mu(1 \mp \gamma_5)$, and α and β are color indices.

The Wilson coefficients from the gluino box contributions are leading contributions when the mass difference between right-handed squarks exists [59, 60]. They are shown in appendix A.1 with their corresponding loop functions defined in appendix B.2.1. Here, $(\delta_d)_{13}(\delta_d)_{32}$ terms are discarded for simplicity.

The Wilson coefficients of the chargino-mediated Z -penguin are induced by terms of second order in the expansion of MIA. These ones are shown in appendix A.2, where the loop function $l(x, y)$ is given by eq. (B.1).

The matching conditions to the standard four-quark Wilson coefficients [37] are

$$\begin{aligned}
s_1 &= 0, & s_2 &= 0, \\
s_3 &= \frac{1}{3} (C_3^u + 2C_3^d), & s_4 &= \frac{1}{3} (C_4^u + 2C_4^d), \\
s_5 &= \frac{1}{3} (C_1^u + 2C_1^d), & s_6 &= \frac{1}{3} (C_2^u + 2C_2^d), \\
s_7 &= \frac{2}{3} (C_1^u - C_1^d), & s_8 &= \frac{2}{3} (C_2^u - C_2^d), \\
s_9 &= \frac{2}{3} (C_3^u - C_3^d), & s_{10} &= \frac{2}{3} (C_4^u - C_4^d).
\end{aligned} \tag{2.45}$$

The coefficients for the opposite-chirality operators, $\tilde{s}_{1,\dots,10}$, are trivially found from the previous ones by replacing $C_{1,2,3,4}^q \rightarrow \tilde{C}_{1,2,3,4}^q$. Using the Wilson coefficients $\vec{s} = (s_1, s_2, \dots, s_{10})^T$ and $\vec{\tilde{s}} = (\tilde{s}_1, \tilde{s}_2, \dots, \tilde{s}_{10})^T$ at the μ^{SUSY} scale, the dominant box and penguin contributions to $\varepsilon'_K/\varepsilon_K$ are given by [37]

$$\left. \frac{\varepsilon'_K}{\varepsilon_K} \right|_{\text{box+pen}} = \frac{G_F \omega_+}{2|\varepsilon_K^{\text{EXP}}| \text{Re}A_0^{\text{EXP}}} \langle \vec{Q}_{\varepsilon'}(\mu)^T \rangle \hat{U}(\mu, \mu^{\text{SUSY}}) \text{Im} \left[\vec{s} - \vec{\tilde{s}} \right], \tag{2.46}$$

with

$$\omega_+ = (4.53 \pm 0.02) \times 10^{-2}, \tag{2.47}$$

$$|\varepsilon_K^{\text{EXP}}| = (2.228 \pm 0.011) \times 10^{-3}, \tag{2.48}$$

$$\text{Re}A_0^{\text{EXP}} = (3.3201 \pm 0.0018) \times 10^{-7} \text{ GeV}. \tag{2.49}$$

The hadronic matrix elements at $\mu = 1.3 \text{ GeV}$, including $I = 0$ and $I = 2$ parts, are [37]

$$\langle \vec{Q}_{\varepsilon'}(\mu)^T \rangle = (0.345, 0.133, 0.034, -0.179, 0.152, 0.288, 2.653, 17.305, 0.526, 0.281) (\text{GeV})^3, \tag{2.50}$$

and the approximate function of the RG evolution matrix $\hat{U}(\mu, \mu^{\text{SUSY}})$ is given in ref. [37].

Next, the $|\Delta S| = 1$ chromomagnetic-dipole operator that contributes to $\varepsilon'_K/\varepsilon_K$ is

$$\mathcal{H}_{\text{eff}} = C_g^- Q_g^- + \text{H.c.}, \tag{2.51}$$

with

$$Q_g^- = -\frac{g_s}{(4\pi)^2} (\bar{s} \sigma^{\mu\nu} T^A \gamma_5 d) G_{\mu\nu}^A. \tag{2.52}$$

The complete expression for the Wilson coefficient C_g^- at the μ^{SUSY} scale is shown in appendix A.3, where $(\delta_d)_{13}(\delta_d)_{32}$ terms are discarded for simplicity. The corresponding loop functions $I(x, y)$, $J(x, y)$, $K(x, y)$, $L(x, y)$, $M_3(x)$, and $M_4(x)$ are defined in appendix B.2.2.

The chromomagnetic-dipole contribution to $\varepsilon'_K/\varepsilon_K$ is [40]

$$\left. \frac{\varepsilon'_K}{\varepsilon_K} \right|_{\text{chromo}} = \frac{\omega_+}{|\varepsilon_K^{\text{EXP}}| \text{Re}A_0^{\text{EXP}}} \left(1 - \hat{\Omega}_{\text{eff}}\right) \frac{11\sqrt{3}}{64\pi^2} \frac{M_\pi^2 M_K^2}{f_\pi(m_s + m_d)} \eta_s B_G \text{Im}C_g^-, \quad (2.53)$$

where $f_\pi = (130.2 \pm 1.7)$ MeV [34], and [52, 61, 62]

$$\hat{\Omega}_{\text{eff}} = 0.148 \pm 0.080, \quad (2.54)$$

$$\eta_s = \left[\frac{\alpha_s(m_b)}{\alpha_s(1.3 \text{ GeV})} \right]^{\frac{2}{25}} \left[\frac{\alpha_s(m_t)}{\alpha_s(m_b)} \right]^{\frac{2}{23}} \left[\frac{\alpha_s(\mu^{\text{SUSY}})}{\alpha_s(m_t)} \right]^{\frac{2}{21}}. \quad (2.55)$$

According to refs. [40, 41], the hadronic matrix element for the chromomagnetic-dipole operator into two pions, B_G , is enhanced by $1/N_c \cdot M_K^2/M_\pi^2$ from the large next-to-leading-order corrections that it receives. Therefore, the leading order in the chiral quark model, $B_G = 1$, is implausible, and we consider $B_G = 1 \pm 3$ in our analyses.

The other contributions are negligible [59]. Note that the sub-leading contributions which come from the gluino-mediated photon-penguin and the chargino-mediated Z -penguins induced by terms of first order in the expansion of the squark mass matrix, have opposite sign and practically cancel each other [59].

Finally, the SUSY contributions to $\varepsilon'_K/\varepsilon_K$ are given as

$$\left(\frac{\varepsilon'_K}{\varepsilon_K} \right)^{\text{SUSY}} \simeq \left. \frac{\varepsilon'_K}{\varepsilon_K} \right|_{\text{box+pen}} + \left. \frac{\varepsilon'_K}{\varepsilon_K} \right|_{\text{chromo}}. \quad (2.56)$$

2.5 ε_K and ΔM_K

Although ε_K is one of the most sensitive quantities to new physics, the SM prediction is still controversial. Especially, the leading short-distance contribution to ε_K in the SM is proportional to $|V_{cb}|^4$ (cf., ref. [63]), whose measured values from inclusive semileptonic B decays ($\bar{B} \rightarrow X_c \ell^- \bar{\nu}$) and from exclusive decays ($\bar{B} \rightarrow D^{(*)} \ell^- \bar{\nu}$ and $\Lambda_b \rightarrow \Lambda_c \ell^- \bar{\nu}$) are inconsistent at a 4.1σ level [35, 64]. A recent discussion about the exclusive $|V_{cb}|$ is given in refs. [65–67].

In this paper, for the SM prediction, we use [36]

$$\varepsilon_K^{\text{SM}} = (2.12 \pm 0.18) \times 10^{-3}, \quad (2.57)$$

with

$$\varepsilon_K = e^{i\varphi_\varepsilon} \varepsilon_K^{\text{SM}}, \quad (2.58)$$

where $\varphi_\varepsilon = \tan^{-1}(2\Delta M_K/\Delta\Gamma_K) = (43.51 \pm 0.05)^\circ$ [34]. This value and the uncertainty are based on the inclusive $|V_{cb}|$ [35], the Wolfenstein parameters in the angle-only-fit method [68], and the long-distance contribution obtained by the lattice simulation [29]. Combining the measured value in eq. (2.48), we impose

$$\varepsilon_K^{\text{EXP/SM}} = 1.05 \pm 0.10(\text{TH}), \quad (2.59)$$

on the χ^2 test, with

$$\varepsilon_K^{\text{SM}} \rightarrow \varepsilon_K^{\text{SM}} + \varepsilon_K^{\text{SUSY}}. \quad (2.60)$$

Note that we also impose $\text{Re}(\varepsilon_K) > 0$ from $\text{Re}(\varepsilon_K) = (1.596 \pm 0.013) \times 10^{-3}$ [69].

Within the MSSM, the SUSY contributions to ε_K are dominated by gluino box diagrams. In this paper, however, we will focus on their suppressed region. The crossed and uncrossed gluino-box diagrams give opposite sign contributions and there is a certain cancellation region [59, 70], and/or simultaneous mixings of (δ_d^{LL}) and (δ_d^{RR}) can also produce the cancellation. Therefore, we also consider the sub-dominant contributions which come from Wino and Higgsino boxes. The $|\Delta S| = 2$ four-quark effective Hamiltonian at the μ^{SUSY} scale is [71]

$$\mathcal{H}_{\text{eff}} = \sum_{i=1}^5 C_i Q_i + \sum_{i=1}^3 \tilde{C}_i \tilde{Q}_i + \text{H.c.}, \quad (2.61)$$

with

$$\begin{aligned} Q_1 &= (\bar{d}\gamma_\mu P_L s) (\bar{d}\gamma^\mu P_L s), & Q_2 &= (\bar{d}P_L s) (\bar{d}P_L s), & Q_3 &= (\bar{d}_\alpha P_L s_\beta) (\bar{d}_\beta P_L s_\alpha), \\ Q_4 &= (\bar{d}P_L s) (\bar{d}P_R s), & Q_5 &= (\bar{d}_\alpha P_L s_\beta) (\bar{d}_\beta P_R s_\alpha), \\ \tilde{Q}_1 &= (\bar{d}\gamma_\mu P_R s) (\bar{d}\gamma^\mu P_R s), & \tilde{Q}_2 &= (\bar{d}P_R s) (\bar{d}P_R s), & \tilde{Q}_3 &= (\bar{d}_\alpha P_R s_\beta) (\bar{d}_\beta P_R s_\alpha). \end{aligned} \quad (2.62)$$

The kaon mixing amplitude $M_{12}^{(K)}$, ΔM_K and ε_K are given by

$$M_{12}^{(K)} = \frac{\langle K^0 | \mathcal{H}_{\text{eff}} | \bar{K}^0 \rangle}{2M_K}, \quad (2.63)$$

$$\Delta M_K = 2\text{Re}[M_{12}^{(K)}], \quad (2.64)$$

$$\varepsilon_K = \kappa_\varepsilon \frac{e^{i\varphi_\varepsilon} \text{Im}[M_{12}^{(K)}]}{\sqrt{2} \Delta M_K^{\text{EXP}}} = e^{i\varphi_\varepsilon} \varepsilon_K^{\text{SUSY}}, \quad (2.65)$$

where $\kappa_\varepsilon = 0.94 \pm 0.02$ [72]. Using the latest lattice result [73], for the hadronic matrix elements, we obtain

$$\langle K^0 | \vec{Q}(\mu) | \bar{K}^0 \rangle = (0.00211, -0.04231, 0.01288, 0.09571, 0.02452) (\text{GeV})^4, \quad (2.66)$$

with $\langle K^0 | \tilde{Q}_{1,2,3}(\mu) | \bar{K}^0 \rangle = \langle K^0 | Q_{1,2,3}(\mu) | \bar{K}^0 \rangle$, where $\mu = 3$ GeV and we used $m_s(\mu) = (81.64 \pm 1.17)$ MeV and $m_d(\mu) = (2.997 \pm 0.049)$ MeV [73].

The leading-order QCD RG corrections are given by [74]

$$C_1(\mu) = \eta_1^K C_1(\mu^{\text{SUSY}}), \quad (2.67)$$

$$\begin{pmatrix} C_2(\mu) \\ C_3(\mu) \end{pmatrix} = X_{23} \eta_{23}^K X_{23}^{-1} \begin{pmatrix} C_2(\mu^{\text{SUSY}}) \\ C_3(\mu^{\text{SUSY}}) \end{pmatrix}, \quad (2.68)$$

$$\begin{pmatrix} C_4(\mu) \\ C_5(\mu) \end{pmatrix} = \begin{pmatrix} (\eta_1^K)^{-4} & \frac{1}{3} [(\eta_1^K)^{-4} - (\eta_1^K)^{\frac{1}{2}}] \\ 0 & (\eta_1^K)^{\frac{1}{2}} \end{pmatrix} \begin{pmatrix} C_4(\mu^{\text{SUSY}}) \\ C_5(\mu^{\text{SUSY}}) \end{pmatrix}, \quad (2.69)$$

with

$$\eta_1^K = \left[\frac{\alpha_s(m_b)}{\alpha_s(\mu)} \right]^{\frac{6}{25}} \left[\frac{\alpha_s(m_t)}{\alpha_s(m_b)} \right]^{\frac{6}{23}} \left[\frac{\alpha_s(\mu^{\text{SUSY}})}{\alpha_s(m_t)} \right]^{\frac{6}{21}}, \quad (2.70)$$

$$\eta_{23}^K = \begin{pmatrix} (\eta_1^K)^{\frac{1}{6}(1-\sqrt{241})} & 0 \\ 0 & (\eta_1^K)^{\frac{1}{6}(1+\sqrt{241})} \end{pmatrix}, \quad (2.71)$$

$$X_{23} = \begin{pmatrix} \frac{1}{2}(-15 - \sqrt{241}) & \frac{1}{2}(-15 + \sqrt{241}) \\ 1 & 1 \end{pmatrix}. \quad (2.72)$$

The QCD corrections to $\tilde{C}_{1,2,3}$ are the same as $C_{1,2,3}$.

The Wilson coefficients from the $|\Delta S| = 2$ gluino boxes are shown in appendix A.4 with their corresponding loop functions defined in appendix B.3.1. In the universal squark mass limit, these results are consistent with ref. [22]. Here, the terms proportional to $[(\mathcal{M}_D^2)_{LR}]_{12}$ or $(\delta_d)_{13}(\delta_d)_{32}$ are discarded for simplicity.

The Wilson coefficients and their corresponding loop functions for the sub-leading contributions to ε_K are given in appendix A.5 and B.3.2, respectively.

3 Parameter scan

The MSSM parameter scan is performed with the framework `Ipanema- β` [75] using a GPU of the model GeForce GTX 1080. The samples are a combination of flat scans plus scans based on genetic algorithms [76]. The cost function used by the genetic algorithm is the likelihood function with the observable constrains. In addition, aiming to get a dense population in regions with $\mathcal{B}(K_S^0 \rightarrow \mu^+ \mu^-)$ significantly different from the SM prediction, specific penalty contributions are added to the total cost function. We also perform specific scans at $\tan \beta \approx 50$ and $M_A \approx 1.6$ TeV as for those values the chances to get sizable MSSM effects are larger.

We study three different scenarios (for the ranges of the scanned parameters see table 2):

- Scenario A: A generic scan with universal gaugino masses. No constraint on the Dark Matter relic density is applied in this case, other than the requirement of neutralino Lightest Supersymmetric Particle (LSP). The LSP is Bino-like in most cases, although some points with Higgsino LSP are also found.
- Scenario B: A scan motivated by scenarios with Higgsino Dark Matter. In this scenario, the relic density is mostly function of the LSP mass, which fulfills the measured density [77] at $m_{\chi_1^0} \approx 1$ TeV [78–81]. Thus, we perform a scan with $|\mu| = 1$ TeV $< M_1$. We assume universal gaugino masses in this scenario, which then implies that $M_3 > 4.5$ TeV.
- Scenario C: A scan motivated by scenarios with Wino Dark Matter, which is possible in mAMSB or pMSSM, although it is under pressure by γ -rays and antiprotons data [82]. In those scenarios, the relic density is mostly function of the LSP mass, which fulfills the experimental value [77] at $m_{\chi_1^0} \approx 3$ TeV [81, 83]. Thus, we make a

Parameter	Scenario A	Scenario B	Scenario C
\tilde{m}_Q	[2, 10]	[2, 10]	[4, 10]
$\tilde{m}_Q^2/\tilde{m}_d^2$	[0.25, 4]	[0.25, 4]	[0.25, 4]
M_3	[2, 10]	[4.5, 15]	[4, 15]
$\tan\beta$	[10, 50]	[10, 50]	[10, 50]
M_A	[1, 2]	[1, 2]	[1, 2]
$ \mu $	[1, 10]	1	[5, 20]
M_1	$\frac{\alpha_1(\mu^{SUSY})}{\alpha_3(\mu^{SUSY})}M_3$	$\frac{\alpha_1(\mu^{SUSY})}{\alpha_3(\mu^{SUSY})}M_3$	5
M_2	$\frac{\alpha_2(\mu^{SUSY})}{\alpha_3(\mu^{SUSY})}M_3$	$\frac{\alpha_2(\mu^{SUSY})}{\alpha_3(\mu^{SUSY})}M_3$	3
B_G	[-2, 4]	[-2, 4]	[-2, 4]
$\text{Re} \left[(\delta_d^{LL(RR)})_{12} \right]$	[-0.2, 0.2]	[-0.2, 0.2]	[-0.2, 0.2]
$\text{Im} \left[(\delta_d^{LL(RR)})_{12} \right]$	[-0.2, 0.2]	[-0.2, 0.2]	[-0.2, 0.2]

Table 2. Scan ranges for scenario A, B (motivated by Higgsino Dark Matter) and C (motivated by Wino Dark Matter). All masses are in TeV. The nuisance parameter B_G appears in the chromomagnetic-dipole contribution to $\varepsilon'_K/\varepsilon_K$.

scan with $M_2 = 3 \text{ TeV} < |\mu|, M_{1,3}$. The Bino mass M_1 is set to 5 TeV for simplicity. Since it is only necessary in order to ensure that the LSP is Wino-like, any other value above 3 TeV (such as, e.g., an mAMSB-like relation $M_1 \approx 9.7 \text{ TeV}$) could also be used without changing the obtained results. The lightest neutralino and the lightest chargino are nearly degenerate, and radiative corrections are expected to bring the chargino mass to be $\approx 160 \text{ MeV}$ heavier than the lightest neutralino [84].

For simplicity, in all cases we set to zero the trilinear couplings and the mass insertions other than $(\delta_d^{LL(RR)})_{12}$ and $(\delta_u^{LL})_{12}$ which is given by the relations in eq. (2.2), and μ is treated as a real parameter, with both signs allowed a priori.

We also perform studies at the MFV limit, using RG equations induced MIs in CMSSM. As expected, no significant effect is found in this case.

For the squark masses, we use $\tilde{m}_Q = \tilde{m}_u \neq \tilde{m}_d$. This set up is motivated by the SUSY SU(5) grand unified theory, where Q and U -squark are contained in $\mathbf{10}$ representation matter multiplet while D -squark is in $\mathbf{\bar{5}}$ representation one. In general, their soft-SUSY breaking masses are different and depend on couplings between the matter multiplets and the SUSY breaking spurion field.

4 Results

In the following, we show the main results of our scans. The points with $\chi^2 < 12.5$, corresponding to 95% C.L. for six degrees of freedom, are considered experimentally viable. The number of degrees of freedom has been calculated as the number of observables, not counting the nuisance parameter B_G , the rigid bound on the $\tan\beta:M_A$ plane, and ΔM_K , which are not Gaussian distributed. Therefore, the χ^2 requirement corresponds to a 95%

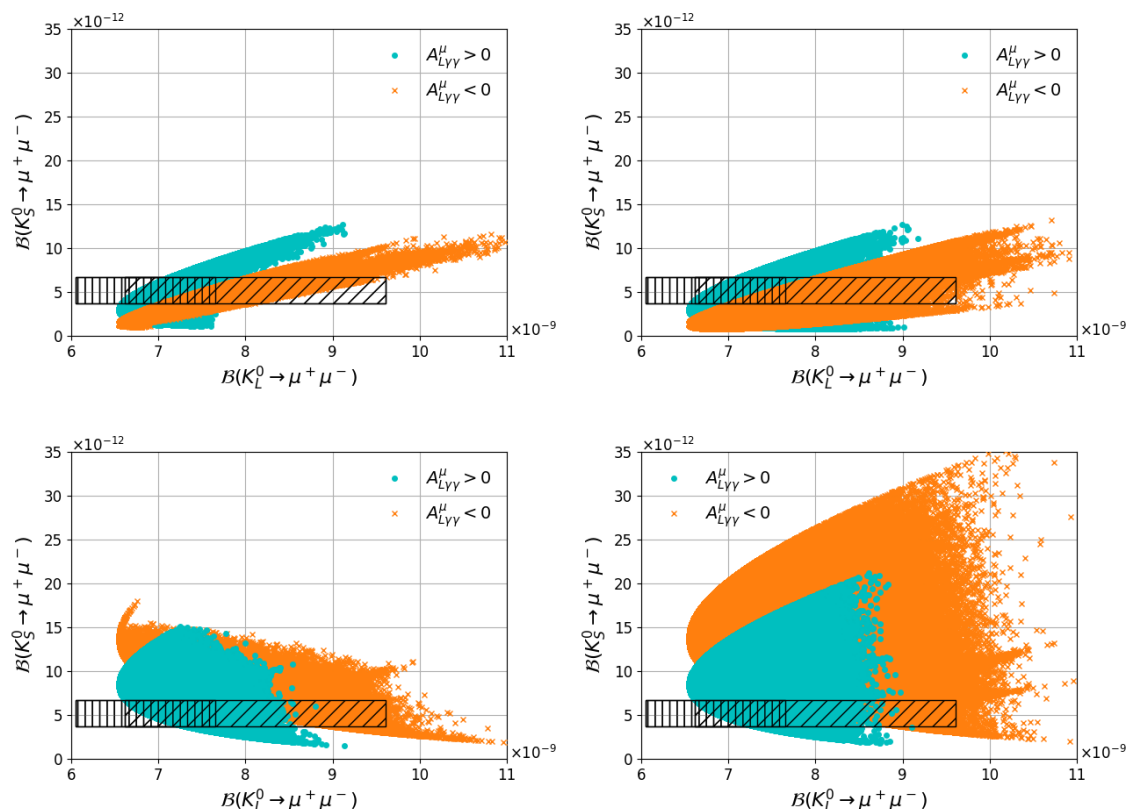


Figure 2. Scenario A $\mathcal{B}(K_S^0 \rightarrow \mu^+\mu^-)$ vs $\mathcal{B}(K_L^0 \rightarrow \mu^+\mu^-)$ for $(\delta_d^{LL})_{12} \neq 0$ and $(M_3 \cdot \mu) > 0$ (upper left), $(\delta_d^{LL})_{12} \neq 0$ and $(M_3 \cdot \mu) < 0$ (upper right), $(\delta_d^{RR})_{12} \neq 0$ and $(M_3 \cdot \mu) > 0$ (lower left), and $(\delta_d^{RR})_{12} \neq 0$ and $(M_3 \cdot \mu) < 0$ (lower right). The cyan dots correspond to $A_{L\gamma\gamma}^\mu > 0$ and the orange crosses to $A_{L\gamma\gamma}^\mu < 0$. The vertically hatched area corresponds to the SM prediction for $A_{L\gamma\gamma}^\mu > 0$ and the inclined hatched area corresponds to the SM prediction for $A_{L\gamma\gamma}^\mu < 0$.

C.L. or tighter. Similar plots are obtained if one uses a looser bound on the absolute χ^2 accompanied with a $\Delta\chi^2 < 5.99$ across the plane being plotted. Due to the large theory uncertainty, $\mathcal{B}(K_L^0 \rightarrow \mu^+\mu^-)$ can go up to $\approx 1 \times 10^{-8}$ at 2σ level. Values slightly above that limit can still be allowed if they reduce the χ^2 contribution in other observables. The allowed regions are separated by the sign of $A_{L\gamma\gamma}^\mu$ in eq. (2.16). We also show results for A_{CP} , which could be experimentally accessed by means of a tagged analysis.

4.1 Effects from $(\delta_d^{LL(RR)})_{12}$ separately

We first study the effects from LL and RR MIs separately. The obtained scatter plots for $\mathcal{B}(K_L^0 \rightarrow \mu^+\mu^-)$ vs $\mathcal{B}(K_S^0 \rightarrow \mu^+\mu^-)$ and $\mathcal{B}(K_S^0 \rightarrow \mu^+\mu^-)$ vs $\varepsilon'_K/\varepsilon_K$ are shown in figure 2 and figure 3 for Scenario A, figure 4 and figure 5 for Scenario B, and figure 6 and figure 7 for Scenario C. The points in the planes correspond to predictions from different values of the input parameters. One should note that in such cases, the SUSY contributions to ε_K can be suppressed naturally in a heavy gluino region ($M_3 \gtrsim 1.5\tilde{m}_Q$) [59, 70].

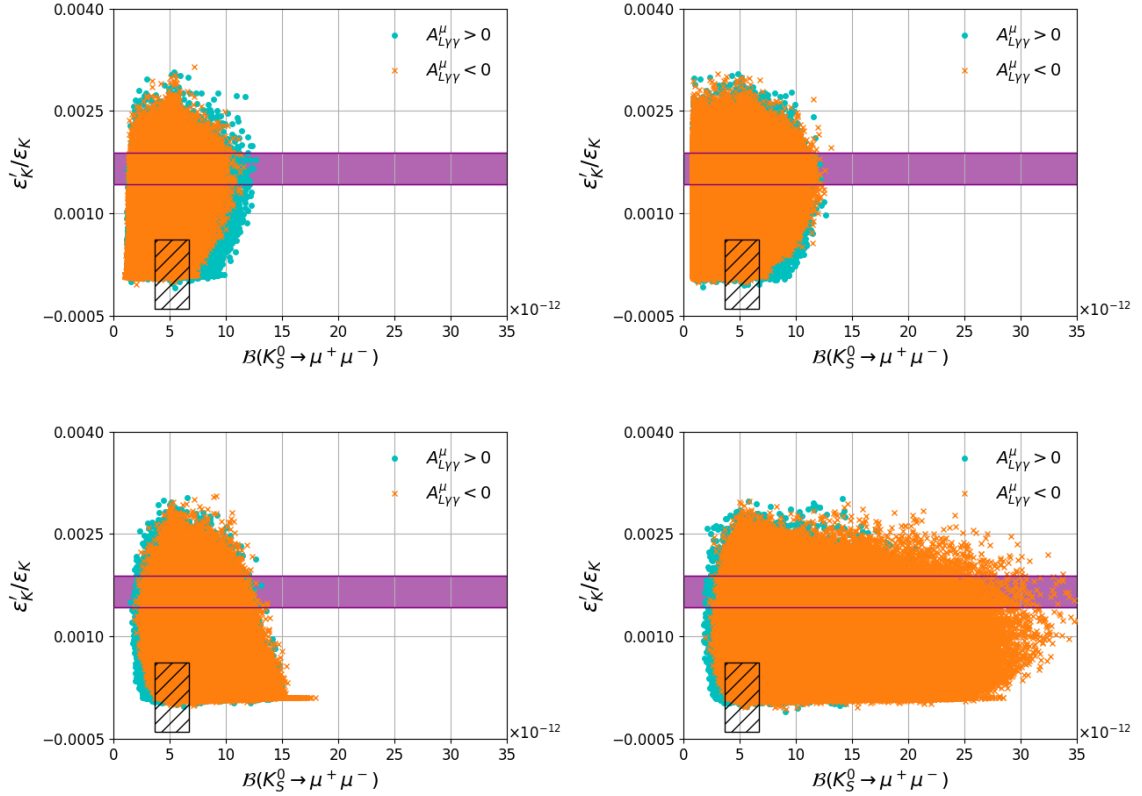


Figure 3. Scenario A $\frac{\epsilon'_K}{\epsilon_K}$ vs $\mathcal{B}(K_S^0 \rightarrow \mu^+ \mu^-)$ for $(\delta_d^{LL})_{12} \neq 0$ and $(M_3 \cdot \mu) > 0$ (upper left), $(\delta_d^{LL})_{12} \neq 0$ and $(M_3 \cdot \mu) < 0$ (upper right), $(\delta_d^{RR})_{12} \neq 0$ and $(M_3 \cdot \mu) > 0$ (lower left), and $(\delta_d^{RR})_{12} \neq 0$ and $(M_3 \cdot \mu) < 0$ (lower right). The cyan dots correspond to $A_{L\gamma\gamma}^\mu > 0$ and the orange crosses to $A_{L\gamma\gamma}^\mu < 0$. The deep purple band corresponds to the experimental results and the hatched area to the SM prediction.

We can see that the allowed 2σ range for $\mathcal{B}(K_S^0 \rightarrow \mu^+ \mu^-)$ is approximately $[0.78, 14] \times 10^{-12}$ for LL -only contributions, and $[1.5, 35] \times 10^{-12}$ for RR -only contributions, without any need of fine-tuning the parameters to avoid constraints from $\mathcal{B}(K_L^0 \rightarrow \mu^+ \mu^-)$. The MSSM contributions are similar for RR and LL , and the differences on the allowed ranges for $\mathcal{B}(K_S^0 \rightarrow \mu^+ \mu^-)$ arise from the interference with the SM amplitudes in $K_{S(L)}^0 \rightarrow \mu^+ \mu^-$, which are shown in section 2.3. It can also be seen that, in Scenario B the maximum departure of $\mathcal{B}(K_S^0 \rightarrow \mu^+ \mu^-)$ from the SM is smaller than in the other scenarios, since $C_{S,P} \propto \mu$ and μ is small relative to squark and gluino masses. The allowed regions for scenarios A and C are very similar to each other, although marginally larger on A. In the contributions to $(\epsilon'_K/\epsilon_K)^{\text{SUSY}}$, the chromomagnetic-dipole contribution can be significant in both LL -only and RR -only cases when $\mu \tan \beta$ and B_G have large values, while the box contributions can be significant only via LL MIs [59]. Note that the penguin contributions to $(\epsilon'_K/\epsilon_K)^{\text{SUSY}}$ are neglected in our parameter scan.

The effective branching fraction and CP asymmetry are shown in figure 8 for Scenario A. Correlation patterns of A_{CP} with other observables can be seen in figure 9, where we

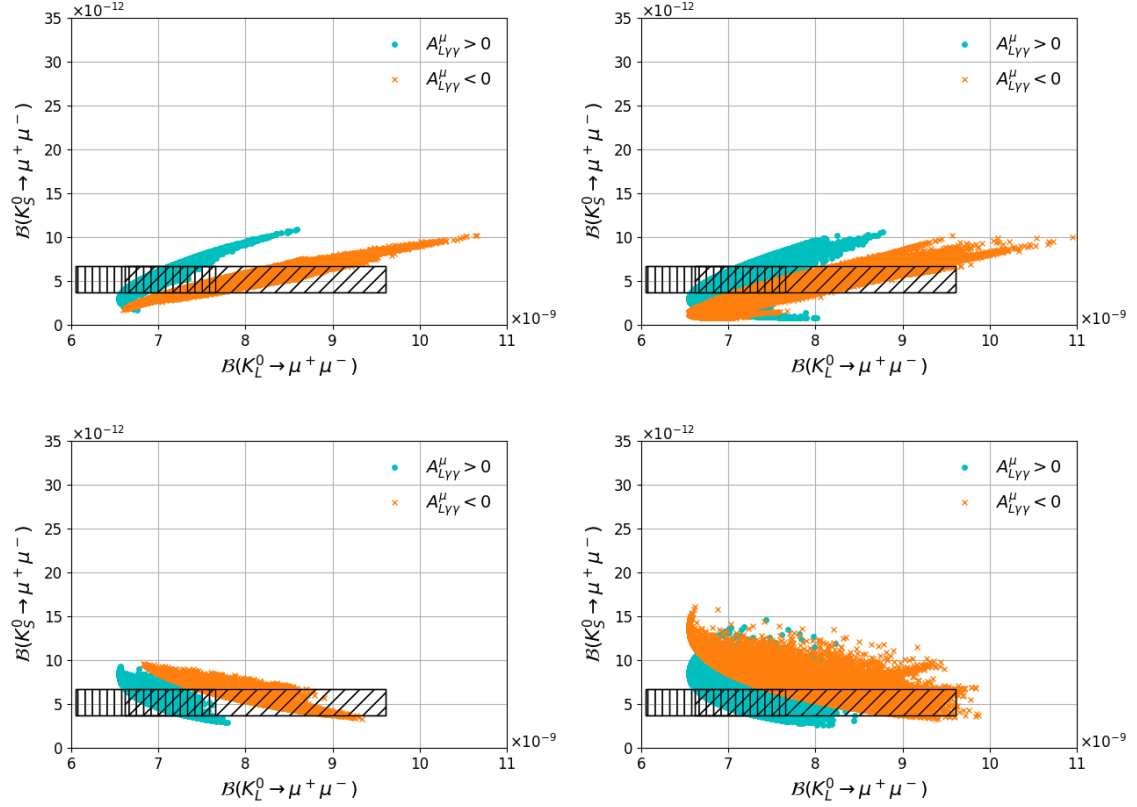


Figure 4. Scenario B, motivated by Higgsino Dark Matter with universal gaugino masses, $\mathcal{B}(K_S^0 \rightarrow \mu^+ \mu^-)$ vs $\mathcal{B}(K_L^0 \rightarrow \mu^+ \mu^-)$ for $(\delta_d^{LL})_{12} \neq 0$ and $(M_3 \cdot \mu) > 0$ (upper left), $(\delta_d^{LL})_{12} \neq 0$ and $(M_3 \cdot \mu) < 0$ (upper right), $(\delta_d^{RR})_{12} \neq 0$ and $(M_3 \cdot \mu) > 0$ (lower left), and $(\delta_d^{RR})_{12} \neq 0$ and $(M_3 \cdot \mu) < 0$ (lower right). The cyan dots correspond to $A_{L\gamma\gamma}^\mu > 0$ and the orange crosses to $A_{L\gamma\gamma}^\mu < 0$. The vertically hatched area corresponds to the SM prediction for $A_{L\gamma\gamma}^\mu > 0$ and the inclined hatched area corresponds to the SM prediction for $A_{L\gamma\gamma}^\mu < 0$.

choose $D' = -D$ and $D = 0.5$ for simplicity. We find that CP asymmetries can be up to ≈ 6 (at $D = 1$), approximately eight times bigger than in the SM. The largest effects are found in left-handed scenarios. Note that the negative value of $\mathcal{B}(K_S^0 \rightarrow \mu^+ \mu^-)_{\text{eff}}$ is cured by inclusion of the background events from $K_L^0 \rightarrow \mu^+ \mu^-$.

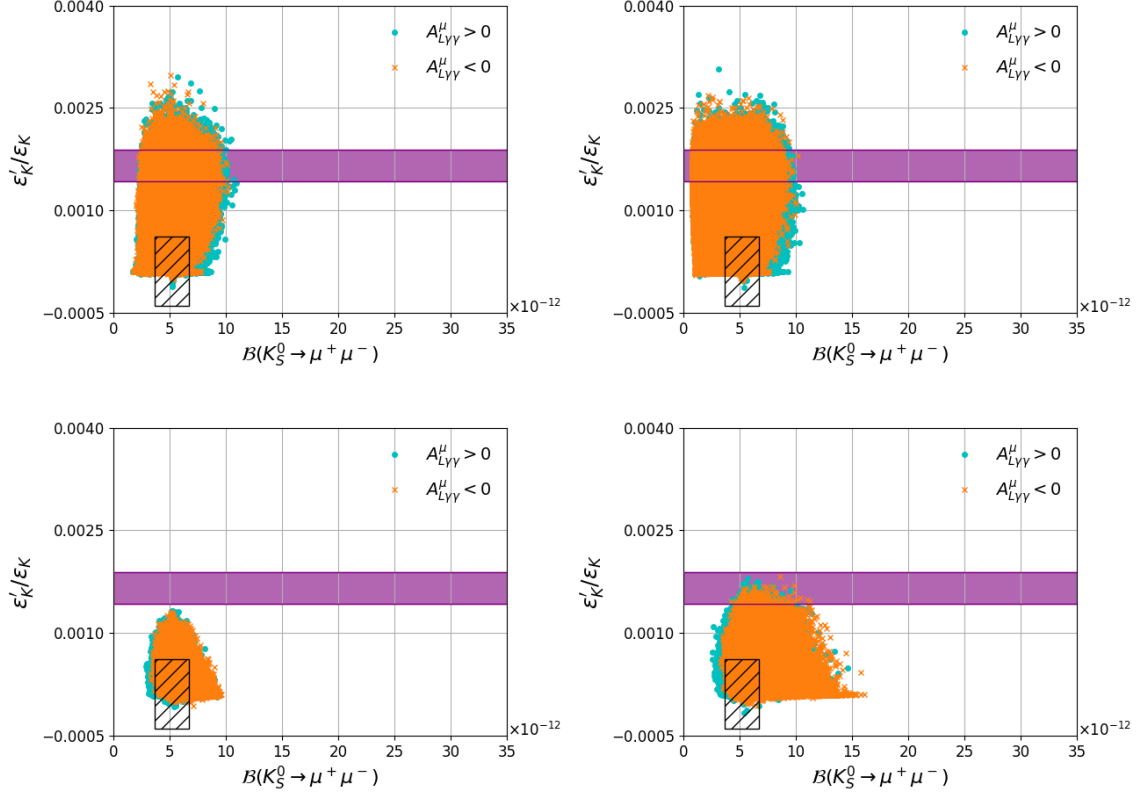


Figure 5. Scenario B, motivated by Higgsino Dark Matter and universal gaugino masses, $\frac{\epsilon'_K}{\epsilon_K}$ vs $\mathcal{B}(K_S^0 \rightarrow \mu^+ \mu^-)$ for $(\delta_d^{LL})_{12} \neq 0$ and $(M_3 \cdot \mu) > 0$ (upper left), $(\delta_d^{LL})_{12} \neq 0$ and $(M_3 \cdot \mu) < 0$ (upper right), $(\delta_d^{RR})_{12} \neq 0$ and $(M_3 \cdot \mu) > 0$ (lower left), and $(\delta_d^{RR})_{12} \neq 0$ and $(M_3 \cdot \mu) < 0$ (lower right). The cyan dots correspond to $A_{L\gamma\gamma}^\mu < 0$ and the orange crosses to $A_{L\gamma\gamma}^\mu > 0$. The deep purple band corresponds to the experimental results and the hatched area to the SM prediction.

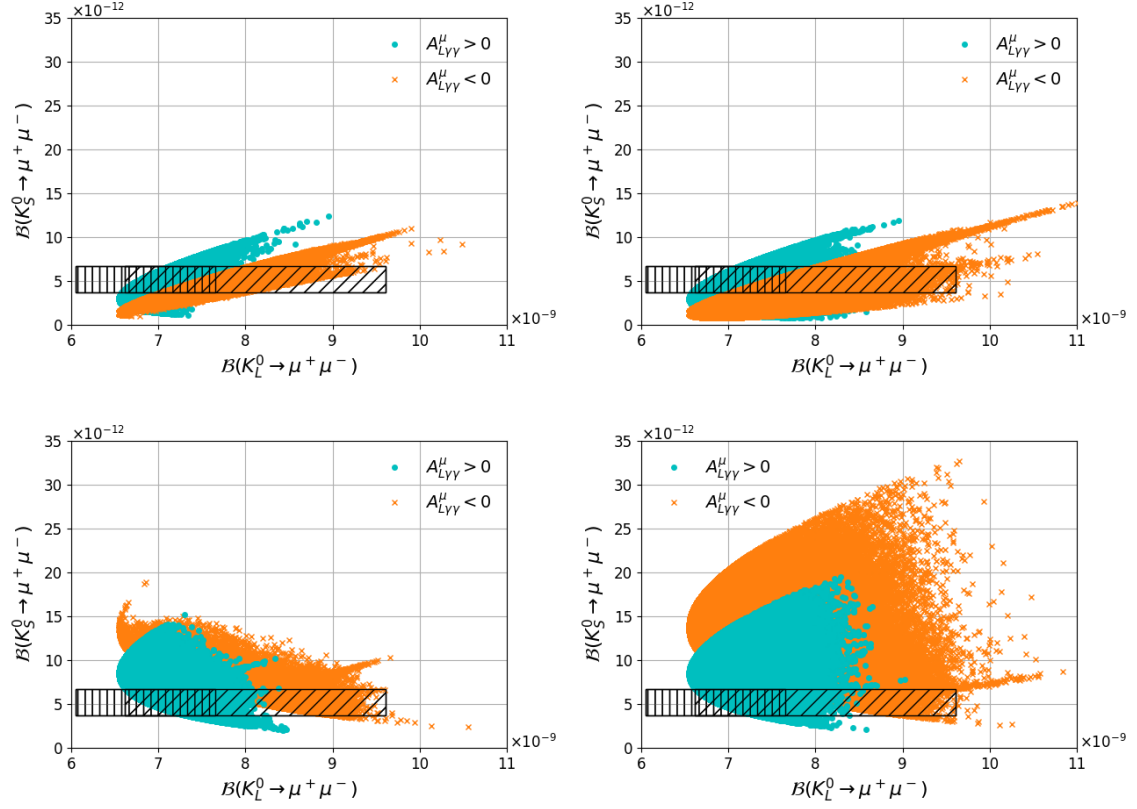


Figure 6. Scenario C (motivated by Wino Dark Matter) $\mathcal{B}(K_S^0 \rightarrow \mu^+ \mu^-)$ vs $\mathcal{B}(K_L^0 \rightarrow \mu^+ \mu^-)$ for $(\delta_d^{LL})_{12} \neq 0$ and $(M_3 \cdot \mu) > 0$ (upper left), $(\delta_d^{LL})_{12} \neq 0$ and $(M_3 \cdot \mu) < 0$ (upper right), $(\delta_d^{RR})_{12} \neq 0$ and $(M_3 \cdot \mu) > 0$ (lower left), and $(\delta_d^{RR})_{12} \neq 0$ and $(M_3 \cdot \mu) < 0$ (lower right). The cyan dots correspond to $A_{L\gamma\gamma}^\mu > 0$ and the orange crosses to $A_{L\gamma\gamma}^\mu < 0$. The vertically hatched area corresponds to the SM prediction for $A_{L\gamma\gamma}^\mu > 0$ and the inclined hatched area corresponds to the SM prediction for $A_{L\gamma\gamma}^\mu < 0$.

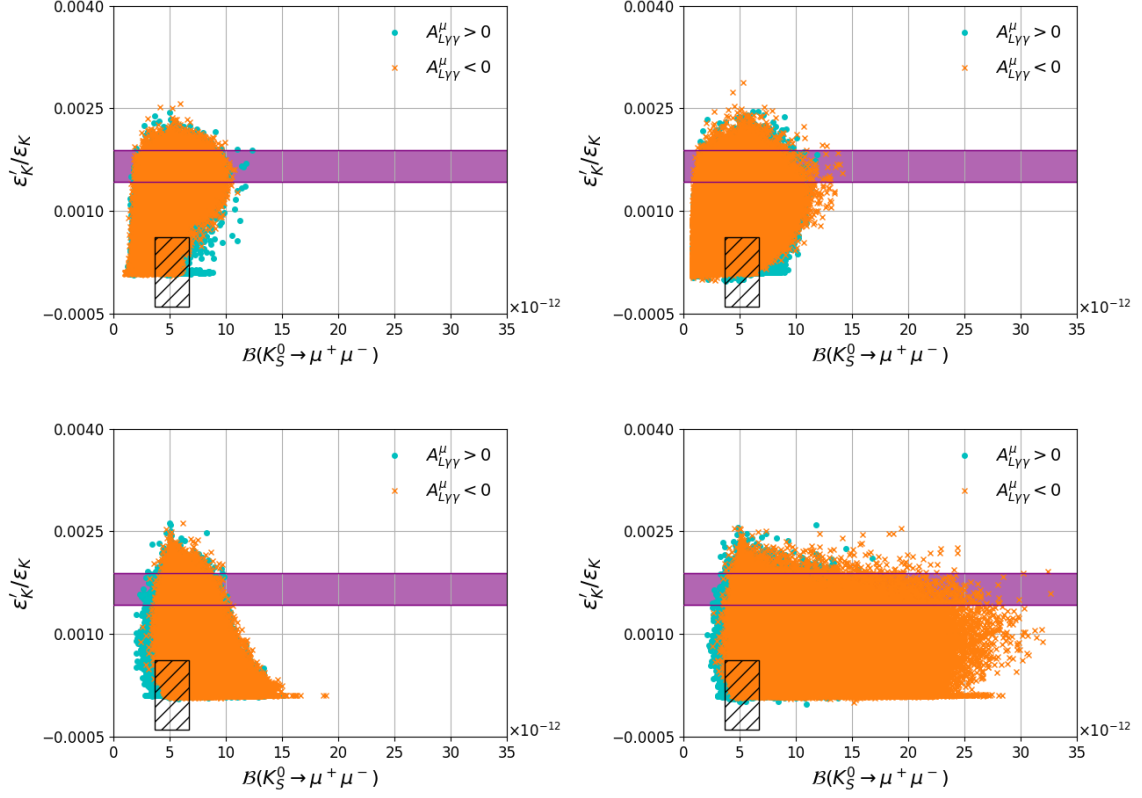


Figure 7. Scenario C, motivated by Wino Dark Matter, $\frac{\epsilon'_K}{\epsilon_K}$ vs $\mathcal{B}(K_S^0 \rightarrow \mu^+\mu^-)$ for $(\delta_d^{LL})_{12} \neq 0$ and $(M_3 \cdot \mu) > 0$ (upper left), $(\delta_d^{LL})_{12} \neq 0$ and $(M_3 \cdot \mu) < 0$ (upper right), $(\delta_d^{RR})_{12} \neq 0$ and $(M_3 \cdot \mu) > 0$ (lower left), and $(\delta_d^{RR})_{12} \neq 0$ and $(M_3 \cdot \mu) < 0$ (lower right). The cyan dots correspond to $A_{L\gamma\gamma}^\mu > 0$ and the orange crosses to $A_{L\gamma\gamma}^\mu < 0$. The deep purple band corresponds to the experimental results and the hatched area to the SM prediction.

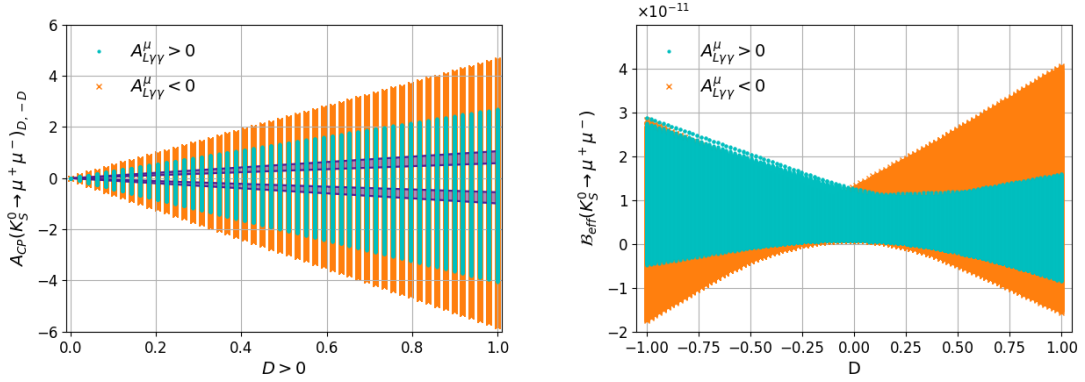


Figure 8. Scenario A, $(\delta_d^{LL})_{12} \neq 0$ and $(M_3 \cdot \mu) < 0$. Plots of $A_{CP}(K_S^0 \rightarrow \mu^+\mu^-)$ vs D (left) for the case $D = -D'$ ($D > 0$) where the cyan dots correspond to $A_{L\gamma\gamma}^\mu > 0$, the orange crosses to $A_{L\gamma\gamma}^\mu < 0$, and the deep purple bands correspond to the SM predictions in eq. (2.31). $B(K_S^0 \rightarrow \mu^+\mu^-)_{\text{eff}}$ vs D (right).

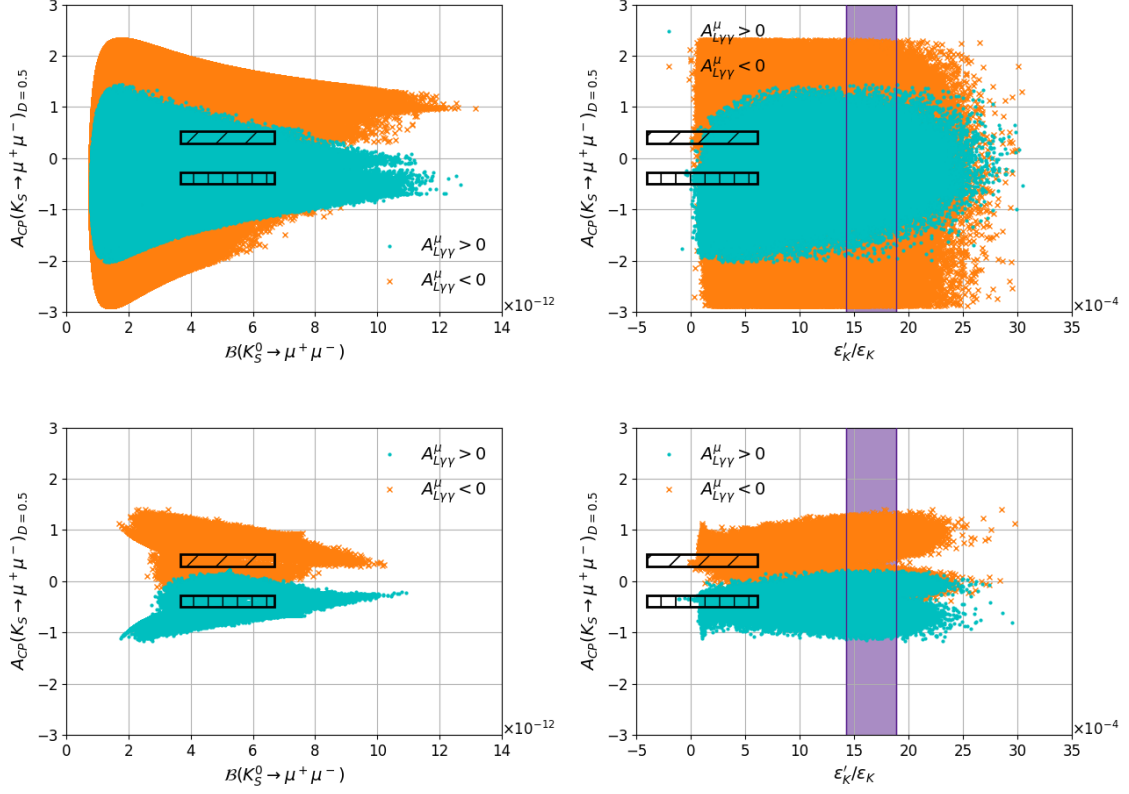


Figure 9. A_{CP} vs $\mathcal{B}(K_S^0 \rightarrow \mu^+ \mu^-)$ (left) and vs $\varepsilon'_K/\varepsilon_K$ (right). The top panels correspond to Scenario A, $(\delta_d^{LL})_{12} \neq 0$ and $(M_3 \cdot \mu) < 0$. The bottom panels correspond to Scenario B, $(\delta_d^{LL})_{12} \neq 0$ and $(M_3 \cdot \mu) > 0$. The plots are done for $D = -D' = 0.5$. The cyan dots correspond to $A_{L\gamma\gamma}^\mu > 0$ and the orange crosses to $A_{L\gamma\gamma}^\mu < 0$. The deep purple bands correspond to the experimental value of $\varepsilon'_K/\varepsilon_K$, the vertically hatched areas correspond to the SM prediction for $A_{L\gamma\gamma}^\mu > 0$ and the inclined hatched areas to the SM prediction for $A_{L\gamma\gamma}^\mu < 0$.

4.2 Floating LL and RR MIs simultaneously

A priori, one possibility to avoid the constraint from $\mathcal{B}(K_L^0 \rightarrow \mu^+ \mu^-)$ is to allow simultaneously for non-zero LL and RR mass insertions. This way both $C_{S(P)}$ and $\tilde{C}_{S(P)}$ are non zero and eqs. (2.17)–(2.22) do not hold. One can then find regions in which the MSSM contributions to $\mathcal{B}(K_S^0 \rightarrow \mu^+ \mu^-)$ do not alter $\mathcal{B}(K_L^0 \rightarrow \mu^+ \mu^-)$ significantly.

For instance, if one chooses

$$\text{Re} [(\delta_d^{LL})_{12}] = -\text{Re} [(\delta_d^{RR})_{12}], \quad \text{Im} [(\delta_d^{LL})_{12}] = \text{Im} [(\delta_d^{RR})_{12}], \quad (4.1)$$

then the SUSY contributions to $\mathcal{B}(K_L^0 \rightarrow \mu^+ \mu^-)$ are canceled, while the SUSY contributions to $\mathcal{B}(K_S^0 \rightarrow \mu^+ \mu^-)$ are maximized (see eqs. (2.9)–(2.13)). However, it is known that in those cases the bounds from ΔM_K and ε_K are very stringent. Using genetic algorithms with cost functions that target large values of $\mathcal{B}(K_S^0 \rightarrow \mu^+ \mu^-)$, we find fine-tuned regions with $\mathcal{B}(K_S^0 \rightarrow \mu^+ \mu^-) > 10^{-10}$, or even at the level of the current experimental bound of 8×10^{-10} at 90% C.L. [19], which are consistent with all our constraints. These points are located along very narrow strips in the $(\delta_d^{LL})_{12}$ vs $(\delta_d^{RR})_{12}$ planes, as shown in figure 10. The figure corresponds to Scenario C as it is the one with higher density of points at large values of $\mathcal{B}(K_S^0 \rightarrow \mu^+ \mu^-)$ and the pattern observed in Scenario A is nearly identical. A particularly favorable region corresponds to the vicinity of eq. (4.1) for $|(\delta_d^{LL})_{12}| \sim 0.03$, with δ_u^{LL} given by the symmetry relation of eq. (2.2). They also favor narrow regions in the squark vs gluino masses planes as shown in figure 4.2. We checked that the values close to the experimental upper bound can still be obtained even if the constraint on ΔM_K is significantly tightened.

We note that the authors in ref. [35] provide a SM prediction for ε_K less consistent with data than the one we used. That prediction is obtained using $|V_{cb}|$ from exclusive decays. If we use that value instead of eq. (2.59),

$$\varepsilon_K^{\text{EXP/SM}} = 1.41 \pm 0.16(\text{TH}), \quad (4.2)$$

then we can accommodate more easily LL and RR MIs of similar sizes, and fine-tuned regions with $\mathcal{B}(K_S^0 \rightarrow \mu^+ \mu^-) > 10^{-10}$ are found with higher chances. The shapes of the strips in the mass insertion planes do not change substantially.

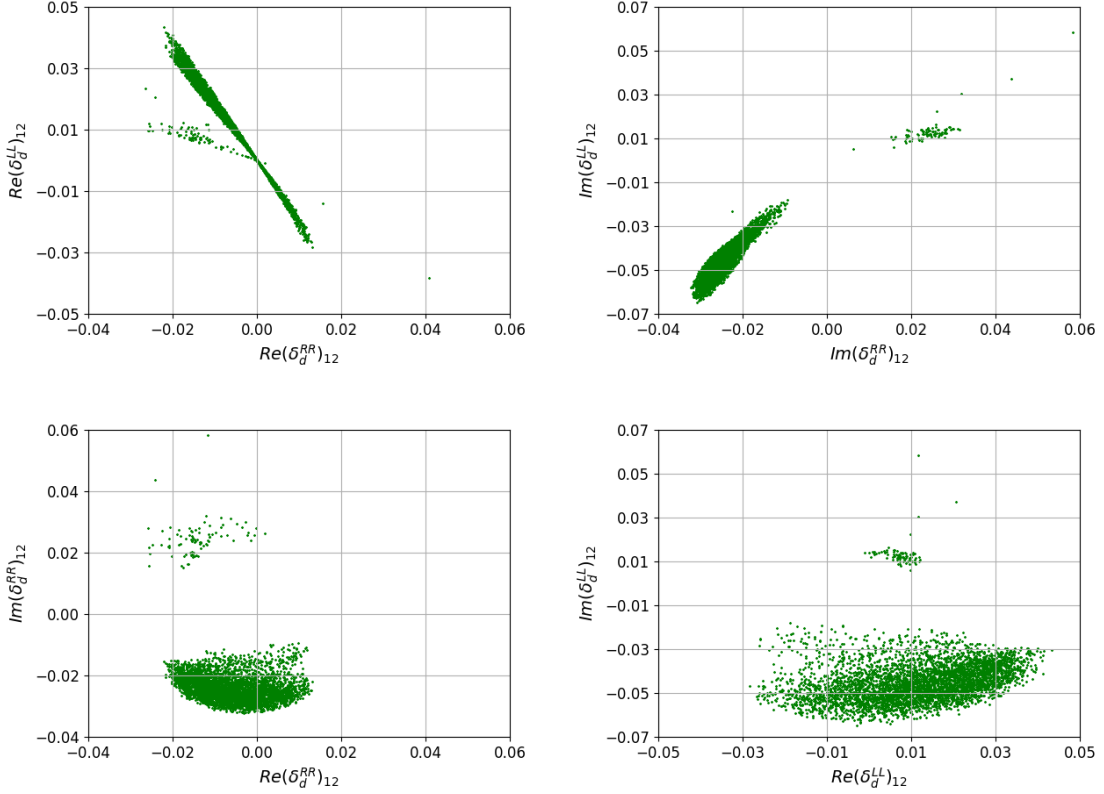


Figure 10. Scatter plots of the real (upper left) and the imaginary (upper right) parts of the mass insertions $(\delta_d^{RR})_{12}$ and $(\delta_d^{LL})_{12}$ for $\mathcal{B}(K_S^0 \rightarrow \mu^+ \mu^-) > 2 \times 10^{-10}$, of the real vs imaginary $(\delta_d^{RR})_{12}$ (lower left) and of the real vs imaginary $(\delta_d^{LL})_{12}$ (lower right). All points in the plane pass the experimental constraints defined in section 2. The up-type MI $(\delta_u^{LL})_{12}$ is given by eq. (2.2). The plots correspond to Scenario C, with a sample of 4378 points with $\mathcal{B}(K_S^0 \rightarrow \mu^+ \mu^-) > 2 \times 10^{-10}$ and $\chi^2 < 12.5$, produced after 6M generations of 200k points each. The pattern observed in Scenario A is very similar.

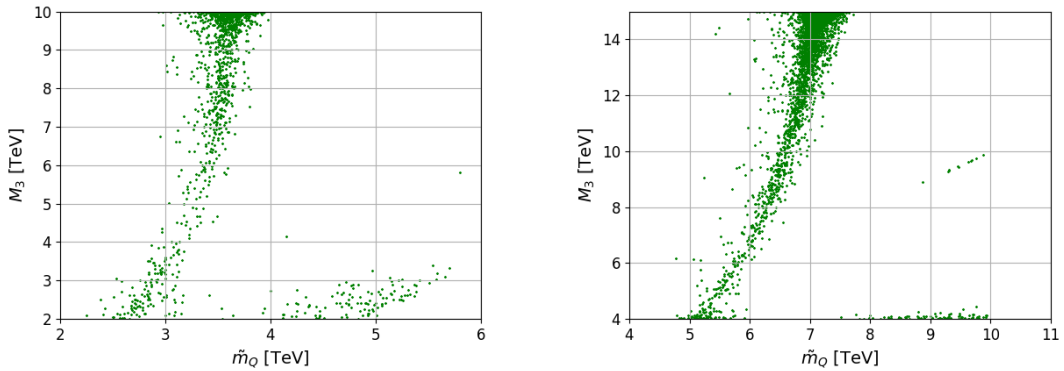


Figure 11. Scatter plot of the squark and gluino masses for $\mathcal{B}(K_S^0 \rightarrow \mu^+ \mu^-) > 2 \times 10^{-10}$ taking into account the constraints defined in section 2. Left: Scenario A, Right: Scenario C. The χ^2 cut in Scenario A has been relaxed to 14 to increase the density of points.

4.3 Non degenerate Higgs masses

The results so far have been obtained in the MSSM framework, in which $|C_S| \approx |C_P|$. This is due to the mass degeneracy $M_H \approx M_A$. In models in which such degeneracy can be broken, the constraint that $\mathcal{B}(K_L^0 \rightarrow \mu^+ \mu^-)$ imposes to $\mathcal{B}(K_S^0 \rightarrow \mu^+ \mu^-)$ relaxes the more those two masses differ. This degeneracy is broken in MSSM at low values of M_A , and requiring $\tan \beta$ to be small to avoid constraints from $\tan \beta : M_A$ planes from LHC. Those regions are more difficult to study, since it would require a detailed specification of the MSSM and test it against bounds of the Higgs sector. The mass degeneracy is also broken in extensions such as NMSSM. According to our scans, on those hypothetical cases one could, in principle reach values of $\mathcal{B}(K_S^0 \rightarrow \mu^+ \mu^-) > 10^{-10}$ for mass differences of $\mathcal{O}(33\%)$ or larger without fine-tuning the MIs.

5 Conclusions

We explored MSSM contribution to $\mathcal{B}(K_S^0 \rightarrow \mu^+ \mu^-)$ for non-zero $(\delta_d^{LL})_{12}$ and $(\delta_d^{RR})_{12}$ mass insertions, motivated by the experimental value of $\varepsilon'_K/\varepsilon_K$, and in the large $\tan \beta$ regime. We find that MSSM contributions to $\mathcal{B}(K_S^0 \rightarrow \mu^+ \mu^-)$ can surpass the SM contributions by up to a factor of seven, reaching the level of 3.5×10^{-11} even for large SUSY masses, with no conflict with existing experimental data. This is also the case even if $\varepsilon'_K/\varepsilon_K$ turns out to be SM-like as predicted by refs. [30–32]. The 3.5×10^{-11} bound is due to the combined effect of $\Delta M_K, \varepsilon_K$, and $K_L^0 \rightarrow \mu^+ \mu^-$ constraints. Such bound is not rigid, and fine-tuned regions can bring the branching fraction above the 10^{-10} level, even up to the current experimental bound; the largest deviations from SM are found at $|(\delta_d^{LL})_{12}| \approx 2|(\delta_d^{RR})_{12}| \sim 0.03$ and $\arg [(\delta_d^{LL})_{12}] \approx -\arg [(\delta_d^{RR})_{12}] + \pi$ for large squark and gluino masses. We also find that the CP asymmetry of $K^0 \rightarrow \mu^+ \mu^-$ can be significantly modified by MSSM contributions, being up to eight times bigger than the SM prediction in the pure LL case. Finally, we remind that, for simplicity, we have restricted our study to the main contributions in the large $\tan \beta$ regime. Discarded terms could, in principle, provide even more flexibility to the allowed regions.

Acknowledgments

We would like to thank G. Isidori, T. Kuwahara, D. Mueller, and K.A. Olive for useful discussions. The research activity of IGFAE/USC members is partially funded by ERC-StG-639068 and partially by XuntaGal. G. D. was supported in part by MIUR under Project No. 2015P5SBHT (PRIN 2015) and by the INFN research initiative ENP.

A Wilson coefficients

A.1 $|\Delta S| = 1$ gluino box contribution

The Wilson coefficients of the gluino box contributions to $\varepsilon'_K/\varepsilon_K$ are

$$\begin{aligned}
C_1^q &= \frac{(\alpha_s)^2}{2\sqrt{2}G_F M_3^2} (\delta_d^{LL})_{12} \left[\frac{1}{18} f(x_3^Q, x_3^q) - \frac{5}{18} g(x_3^Q, x_3^q) \right], \\
C_2^q &= \frac{(\alpha_s)^2}{2\sqrt{2}G_F M_3^2} (\delta_d^{LL})_{12} \left[\frac{7}{6} f(x_3^Q, x_3^q) + \frac{1}{6} g(x_3^Q, x_3^q) \right], \\
C_3^q &= \frac{(\alpha_s)^2}{2\sqrt{2}G_F M_3^2} (\delta_d^{LL})_{12} \left[-\frac{5}{9} f(x_3^Q, x_3^Q) + \frac{1}{36} g(x_3^Q, x_3^Q) \right], \\
C_4^q &= \frac{(\alpha_s)^2}{2\sqrt{2}G_F M_3^2} (\delta_d^{LL})_{12} \left[\frac{1}{3} f(x_3^Q, x_3^Q) + \frac{7}{12} g(x_3^Q, x_3^Q) \right], \\
\tilde{C}_1^q &= \frac{(\alpha_s)^2}{2\sqrt{2}G_F M_3^2} (\delta_d^{RR})_{12} \left[\frac{1}{18} f(x_3^d, x_3^Q) - \frac{5}{18} g(x_3^d, x_3^Q) \right], \\
\tilde{C}_2^q &= \frac{(\alpha_s)^2}{2\sqrt{2}G_F M_3^2} (\delta_d^{RR})_{12} \left[\frac{7}{6} f(x_3^d, x_3^Q) + \frac{1}{6} g(x_3^d, x_3^Q) \right], \\
\tilde{C}_3^q &= \frac{(\alpha_s)^2}{2\sqrt{2}G_F M_3^2} (\delta_d^{RR})_{12} \left[-\frac{5}{9} f(x_3^d, x_3^q) + \frac{1}{36} g(x_3^d, x_3^q) \right], \\
\tilde{C}_4^q &= \frac{(\alpha_s)^2}{2\sqrt{2}G_F M_3^2} (\delta_d^{RR})_{12} \left[\frac{1}{3} f(x_3^d, x_3^q) + \frac{7}{12} g(x_3^d, x_3^q) \right], \tag{A.1}
\end{aligned}$$

where q runs u and d , and $x_3^Q = \tilde{m}_Q^2/M_3^2$ and $x_3^q = \tilde{m}_q^2/M_3^2$.

A.2 $|\Delta S| = 1$ chargino-mediated Z-penguin contribution

The Wilson coefficients of the chargino-mediated Z-penguin are

$$\begin{aligned}
C_1^u &= -\frac{(\alpha_2)^2 \sin^2 \theta_W}{12\sqrt{2}G_F M_W^2} \frac{[(\mathcal{M}_U^2)_{LR}]_{23}^* [(\mathcal{M}_U^2)_{LR}]_{13}}{M_2^4} l(x_2^Q, x_2^u), \\
C_1^d &= \frac{(\alpha_2)^2 \sin^2 \theta_W}{24\sqrt{2}G_F M_W^2} \frac{[(\mathcal{M}_U^2)_{LR}]_{23}^* [(\mathcal{M}_U^2)_{LR}]_{13}}{M_2^4} l(x_2^Q, x_2^u), \\
C_3^u &= \frac{(\alpha_2)^2}{16\sqrt{2}G_F M_W^2} \left(1 - \frac{4}{3} \sin^2 \theta_W\right) \frac{[(\mathcal{M}_U^2)_{LR}]_{23}^* [(\mathcal{M}_U^2)_{LR}]_{13}}{M_2^4} l(x_2^Q, x_2^u), \\
C_3^d &= -\frac{(\alpha_2)^2}{16\sqrt{2}G_F M_W^2} \left(1 - \frac{2}{3} \sin^2 \theta_W\right) \frac{[(\mathcal{M}_U^2)_{LR}]_{23}^* [(\mathcal{M}_U^2)_{LR}]_{13}}{M_2^4} l(x_2^Q, x_2^u), \\
C_{2,4}^q &= \tilde{C}_{1,2,3,4}^q = 0. \tag{A.2}
\end{aligned}$$

A.3 $|\Delta S| = 1$ chromomagnetic dipole contribution

The Wilson coefficients of the chromomagnetic dipole contributions to $\varepsilon'_K/\varepsilon_K$ are

$$\begin{aligned}
C_g^- &= \frac{\alpha_s \pi}{3} \frac{\tilde{m}_Q^2 \mu m_s}{M_3^5} (\delta_d^{LL})_{12} \frac{\tan \beta}{1 + \epsilon_g \tan \beta} \left[I(x_3^Q, x_3^d) + 9J(x_3^Q, x_3^d) \right] \\
&\quad - \frac{\alpha_s \pi}{3} \frac{\tilde{m}_d^2 \mu m_s}{M_3^5} (\delta_d^{RR})_{12} \frac{\tan \beta}{1 + \epsilon_g \tan \beta} \left[I(x_3^d, x_3^Q) + 9J(x_3^d, x_3^Q) \right] \\
&\quad + \frac{\alpha_s \pi}{3} \frac{[(\mathcal{M}_D^2)_{LR}]_{12} - [(\mathcal{M}_D^2)_{LR}]_{21}^*}{M_3^3} \left[K(x_3^Q, x_3^d) + 9L(x_3^Q, x_3^d) \right] \\
&\quad - \frac{\alpha_s \pi}{3} \frac{m_s}{\tilde{m}_Q^2} (\delta_d^{LL})_{12} [M_3(x_Q^3) + 9M_4(x_Q^3)] \\
&\quad + \frac{\alpha_s \pi}{3} \frac{m_s}{\tilde{m}_d^2} (\delta_d^{RR})_{12} [M_3(x_d^3) + 9M_4(x_d^3)].
\end{aligned} \tag{A.3}$$

A.4 $|\Delta S| = 2$ gluino box contribution

The Wilson coefficients of the gluino box contributions to ε_K are

$$C_1 = -\frac{(\alpha_s)^2}{\tilde{m}_Q^2} [(\delta_d^{LL})_{21}]^2 g_1^{(1)}(x_Q^3), \tag{A.4}$$

$$C_4 = -\frac{(\alpha_s)^2}{M_3^2} [(\delta_d^{LL})_{21} (\delta_d^{RR})_{21}] g_4^{(1)}(x_Q^3, x_d^3), \tag{A.5}$$

$$C_5 \simeq -\frac{(\alpha_s)^2}{M_3^2} [(\delta_d^{LL})_{21} (\delta_d^{RR})_{21}] g_5^{(1)}(x_Q^3, x_d^3), \tag{A.6}$$

$$\tilde{C}_1 = -\frac{(\alpha_s)^2}{\tilde{m}_d^2} [(\delta_d^{RR})_{21}]^2 g_1^{(1)}(x_d^3), \tag{A.7}$$

$$C_2 = C_3 = \tilde{C}_2 = \tilde{C}_3 = 0. \tag{A.8}$$

A.5 Sub-leading contributions to ε_K

The Wilson coefficients of the Wino and Higgsino contributions are

$$\begin{aligned}
C_1 &= -\frac{\alpha_s \alpha_2}{6 \tilde{m}_Q^2} [(\delta_d^{LL})_{21}]^2 g_{\tilde{g}\tilde{w}}^{(1)}(x_Q^3, x_Q^2) - \frac{(\alpha_2)^2}{8 \tilde{m}_Q^2} [(\delta_d^{LL})_{21}]^2 g_{\tilde{w}}^{(1)}(x_Q^2) \\
&\quad - \frac{(\alpha_2)^2}{8 \tilde{m}_u^2} (V_{ts} V_{td}^*)^2 \frac{m_t^4}{M_W^4} f_1(x_u^\mu),
\end{aligned} \tag{A.9}$$

$$\tilde{C}_3 = -\frac{(\alpha_2)^2}{8} (V_{ts} V_{td}^*)^2 \frac{m_s^2 \tan^2 \beta}{(1 + \epsilon_g \tan \beta)^2} \frac{m_t^4}{M_W^4} \frac{\mu^2 A_t^2}{\tilde{m}_Q^4 \tilde{m}_u^4} f_3(x_Q^\mu, x_u^\mu), \tag{A.10}$$

$$C_2 = C_3 = C_4 = C_5 = \tilde{C}_1 = \tilde{C}_2 = 0. \tag{A.11}$$

Note that a $\tan^4 \beta$ enhanced contribution to ε_K comes from the exchange of neutral Higgses, which is discarded because of $(\delta_d)_{23} (\delta_d)_{31} = 0$ in our analyses. For the Wilson

coefficient, we obtain

$$C_2 \simeq \tilde{C}_2 \simeq 0, \quad (\text{A.12})$$

$$C_4 \simeq -\frac{8(\alpha_s)^2 \alpha_2}{9\pi} \frac{m_b^2}{M_W^2} \frac{\tan^4 \beta}{(1 + \epsilon_g \tan \beta)^2 [1 + (\epsilon_g + \epsilon_Y y_t^2) \tan \beta]^2} \frac{\mu^2 M_3^2}{M_A^2 \tilde{m}_Q^2 \tilde{m}_d^2} \\ \times [(\delta_d^{LL})_{23} (\delta_d^{LL})_{31} (\delta_d^{RR})_{23} (\delta_d^{RR})_{31}] H(x_Q^3, x_d^d) H(x_d^3, x_d^Q), \quad (\text{A.13})$$

$$C_1 = C_3 = C_5 = \tilde{C}_1 = \tilde{C}_3 = 0, \quad (\text{A.14})$$

where the approximation in eq. (2.39) is used, and the loop function $H(x, y)$ is given in eq. (B.4). Note that the CP -even and CP -odd Higgs contributions to C_2 (\tilde{C}_2) are canceled out by each other.

B Loop functions

B.1 $K^0 \rightarrow \mu^+ \mu^-$

The loop functions $l(x, y)$, $F(x, y)$, $G(x, y)$, and $H(x, y)$ are given by

$$l(x, y) = -\frac{[x^2 + (x-2)y] x \ln x}{(x-1)^2(x-y)^3} + \frac{[y^2 + (y-2)x] y \ln y}{(y-1)^2(x-y)^3} - \frac{x+y-2xy}{(x-1)(y-1)(x-y)^2}, \quad (\text{B.1})$$

$$F(x, y) = \frac{x \ln x}{(x-1)(x-y)} + \frac{y \ln y}{(y-1)(y-x)}, \quad (\text{B.2})$$

$$G(x, y) = \frac{x \ln x}{(x-1)^2(x-y)} + \frac{y \ln y}{(y-1)^2(y-x)} + \frac{1}{(x-1)(y-1)}, \quad (\text{B.3})$$

$$H(x, y) = \frac{x \ln x}{(x-1)^2(x-y)^2} + \frac{(x+xy-2y^2) \ln y}{(y-1)^3(x-y)^2} - \frac{2x-y-1}{(x-1)(y-1)^2(x-y)}, \quad (\text{B.4})$$

where $l(1, 1) = -1/12$, $F(1, 1) = 1/2$, $G(1, 1) = -1/6$, and $H(1, 1) = 1/12$.

B.2 ϵ'_K/ϵ_K

B.2.1 $|\Delta S| = 1$ gluino box contributions

The loop functions $f(x, y)$ and $g(x, y)$ [60] are

$$f(x, y) = \frac{x[2x^2 - (x+1)y] \ln x}{(x-1)^3(x-y)^2} - \frac{xy \ln y}{(y-1)^2(x-y)^2} + \frac{x(x+1-2y)}{(x-1)^2(y-1)(x-y)}, \quad (\text{B.5})$$

$$g(x, y) = -\frac{x^2[x(x+1) - 2y] \ln x}{(x-1)^3(x-y)^2} + \frac{xy^2 \ln y}{(y-1)^2(x-y)^2} + \frac{x[-2x + (x+1)y]}{(x-1)^2(y-1)(x-y)}, \quad (\text{B.6})$$

which lead to

$$f(x, x) = -\frac{1+4x-5x^2+2x(2+x) \ln x}{2(x-1)^4} = \frac{1}{x} B_2 \left(\frac{1}{x} \right), \quad (\text{B.7})$$

$$g(x, x) = \frac{x[5-4x-x^2+2(1+2x) \ln x]}{2(x-1)^4} = -\frac{4}{x} B_1 \left(\frac{1}{x} \right). \quad (\text{B.8})$$

The loop functions $B_{1,2}(x)$ are consistent with ref. [71] for the universal squark masses case.

B.2.2 Chromomagnetic-dipole operator

The loop functions $I(x, y)$, $J(x, y)$, $K(x, y)$, $L(x, y)$, $M_3(x)$, and $M_4(x)$ are given by

$$I(x, y) = \frac{(3x^2 - y - 2xy) \ln x}{(x-1)^4(x-y)^2} - \frac{y \ln y}{(y-1)^3(x-y)^2} + \frac{-2 + (-5+x)x + 9y + (2+x)xy - (5+x)y^2}{2(x-y)(x-1)^3(y-1)^2}, \quad (\text{B.9})$$

$$J(x, y) = -\frac{x[(1+2x)x - (2+x)y] \ln x}{(x-1)^4(x-y)^2} + \frac{y^2 \ln y}{(y-1)^3(x-y)^2} + \frac{(5+x)x - 3y(1+x)^2 + (1+5x)y^2}{2(x-1)^3(y-1)^2(x-y)}, \quad (\text{B.10})$$

$$K(x, y) = \frac{x \ln x}{(x-y)(x-1)^3} + \frac{y \ln y}{(y-x)(y-1)^3} + \frac{xy + x + y - 3}{2(x-1)^2(y-1)^2}, \quad (\text{B.11})$$

$$L(x, y) = -\frac{x^2 \ln x}{(x-y)(x-1)^3} - \frac{y^2 \ln y}{(y-x)(y-1)^3} + \frac{1+x+y-3xy}{2(x-1)^2(y-1)^2}, \quad (\text{B.12})$$

$$M_3(x) = \frac{-1 + 9x + 9x^2 - 17x^3 + 6x^2(3+x) \ln x}{12(x-1)^5}, \quad (\text{B.13})$$

$$M_4(x) = \frac{-1 - 9x + 9x^2 + x^3 - 6x(1+x) \ln x}{6(x-1)^5}, \quad (\text{B.14})$$

which lead to

$$K(x, x) = \frac{-5 + 4x + x^2 - 2(1+2x) \ln x}{2(x-1)^4} = \frac{1}{x^2} M_1 \left(\frac{1}{x} \right), \quad (\text{B.15})$$

$$L(x, x) = \frac{1 + 4x - 5x^2 + 2x(2+x) \ln x}{2(x-1)^4} = -\frac{1}{x} B_2 \left(\frac{1}{x} \right). \quad (\text{B.16})$$

The above $M_{1,3,4}(x)$ are consistent with ref. [71] in the universal squark masses case.^{#6}

B.3 ϵ_K

B.3.1 $|\Delta S| = 2$ gluino box contributions

The loop functions $g_1^{(1)}(x)$, $g_4^{(1)}(x, y)$, and $g_5^{(1)}(x, y)$ are given by

$$g_1^{(1)}(x) = -\frac{11 + 144x + 27x^2 - 2x^3}{108(1-x)^4} - \frac{x(13 + 17x)}{18(1-x)^5} \ln x, \quad (\text{B.17})$$

$$g_4^{(1)}(x, y) = -\frac{x^2 y \ln x}{3(x-y)^3(1-x)^3} \{x^2(5+7x) + y[2+7(x-3)x]\} - \frac{y^2 x \ln y}{3(y-x)^3(1-y)^3} \{y^2(5+7y) + x[2+7(y-3)y]\} + \frac{xy}{3(1-x)^2(1-y)^2(x-y)^2} (x+y-13x^2-13y^2+8xy+15x^2y+15xy^2-14x^2y^2), \quad (\text{B.18})$$

^{#6} We found that in eq. (14) of ref. [71], $M_2(x) = -xB_2(x)$ should be replaced by $M_2(x) = -B_2(x)/x$, which has been pointed out in ref. [85].

$$\begin{aligned}
g_5^{(1)}(x, y) = & -\frac{x^2 y \ln x}{9(x-y)^3(1-x)^3} [x^2(11+x) + (x-5)(x+2)y] \\
& -\frac{y^2 x \ln y}{9(y-x)^3(1-y)^3} [y^2(11+y) + (y-5)(y+2)x] \\
& -\frac{xy}{9(1-x)^2(1-y)^2(x-y)^2} (5x + 5y + 7x^2 + 7y^2 - 32xy + 3x^2y + 3xy^2 + 2x^2y^2).
\end{aligned} \tag{B.19}$$

B.3.2 Wino and Higgsino contributions

The loop functions $g_{\tilde{g}\tilde{w}}^{(1)}$, $g_{\tilde{w}}^{(1)}(x)$, $f_1(x)$ and $f_3(x, y)$ are given by

$$\begin{aligned}
g_{\tilde{g}\tilde{w}}^{(1)}(x, y) = & -\sqrt{xy} \left[\frac{x \ln x}{(x-y)(1-x)^4} + \frac{y \ln y}{(y-x)(1-y)^4} \right. \\
& \left. + \frac{11 - 7(x+y) + 2(x^2 + y^2) - 10xy + 5xy(x+y) - x^2y^2}{6(1-x)^3(1-y)^3} \right] \\
& -\frac{x^2 \ln x}{2(x-y)(1-x)^4} - \frac{y^2 \ln y}{2(y-x)(1-y)^4} \\
& -\frac{2 + 5(x+y) - (x^2 + y^2) - 22xy + 5xy(x+y) + 2x^2y^2}{12(1-x)^3(1-y)^3},
\end{aligned} \tag{B.20}$$

$$g_{\tilde{w}}^{(1)}(x) = \frac{-5 - 67x - 13x^2 + x^3}{12(1-x)^4} - \frac{x(3+4x)}{(1-x)^5} \ln x, \tag{B.21}$$

$$f_1(x) = -\frac{x+1}{4(1-x)^2} - \frac{x}{2(1-x)^3} \ln x, \tag{B.22}$$

$$\begin{aligned}
f_3(x, y) = & -\frac{x^2[x(1+x+y) - 3y]}{(x-y)^3(1-x)^3} \ln x - \frac{y^2[y(1+x+y) - 3x]}{(y-x)^3(1-y)^3} \ln y \\
& - 2\frac{x^2 + y^2 - xy - x^2y - xy^2 + x^2y^2}{(1-x)^2(1-y)^2(x-y)^2},
\end{aligned} \tag{B.23}$$

$$f_3(x) = \frac{x^2 - 8x - 17}{6(1-x)^4} - \frac{3x+1}{(1-x)^5} \ln x, \tag{B.24}$$

where $\lim_{y \rightarrow x} f_3(x, y) = f_3(x)$.^{#7}

References

- [1] C. Hamzaoui, M. Pospelov, and M. Toharia, ‘‘Higgs mediated FCNC in supersymmetric models with large $\tan\beta$,’’ *Phys. Rev.* **D59** (1999) 095005, [arXiv:hep-ph/9807350](#) [[hep-ph](#)].
- [2] K. S. Babu and C. F. Kolda, ‘‘Higgs mediated $B^0 \rightarrow \mu^+\mu^-$ in minimal supersymmetry,’’ *Phys. Rev. Lett.* **84** (2000) 228–231, [arXiv:hep-ph/9909476](#) [[hep-ph](#)].
- [3] P. H. Chankowski and L. Slawianowska, ‘‘ $B_{d,s}^0 \rightarrow \mu^-\mu^+$ decay in the MSSM,’’ *Phys. Rev.* **D63** (2001) 054012, [arXiv:hep-ph/0008046](#) [[hep-ph](#)].
- [4] C. Bobeth, T. Ewerth, F. Kruger, and J. Urban, ‘‘Analysis of neutral Higgs boson contributions to the decays $\bar{B}(s) \rightarrow \ell^+\ell^-$ and $\bar{B} \rightarrow K\ell^+\ell^-$,’’ *Phys. Rev.* **D64** (2001) 074014, [arXiv:hep-ph/0104284](#) [[hep-ph](#)].

^{#7} We found that in eq. (A.15) in ref. [22], $f_3(x) = (x^2 - 6x - 17)/[6(1-x)^4] - (3x+1)\ln x/(1-x)^5$ should be replaced by eq. (B.24).

- [5] G. Isidori and A. Retico, “Scalar flavor changing neutral currents in the large $\tan\beta$ limit,” *JHEP* **11** (2001) 001, [arXiv:hep-ph/0110121 \[hep-ph\]](#).
- [6] G. Isidori and A. Retico, “ $B_{s,d} \rightarrow \ell^+\ell^-$ and $K_L \rightarrow \ell^+\ell^-$ in SUSY models with nonminimal sources of flavor mixing,” *JHEP* **09** (2002) 063, [arXiv:hep-ph/0208159 \[hep-ph\]](#).
- [7] S. R. Choudhury and N. Gaur, “Dileptonic decay of B_s meson in SUSY models with large $\tan\beta$,” *Phys. Lett.* **B451** (1999) 86–92, [arXiv:hep-ph/9810307 \[hep-ph\]](#).
- [8] C.-S. Huang, W. Liao, Q.-S. Yan, and S.-H. Zhu, “ $B_s \rightarrow$ lepton + lepton - in a general 2 HDM and MSSM,” *Phys. Rev.* **D63** (2001) 114021, [arXiv:hep-ph/0006250 \[hep-ph\]](#). [Erratum: *Phys. Rev.*D64,059902(2001)].
- [9] Z. Xiong and J. M. Yang, “ B meson dileptonic decays enhanced by supersymmetry with large $\tan\beta$,” *Nucl. Phys.* **B628** (2002) 193–216, [arXiv:hep-ph/0105260 \[hep-ph\]](#).
- [10] A. Dedes, H. K. Dreiner, and U. Nierste, “Correlation of $B_s \rightarrow \mu^+\mu^-$ and $(g-2) (\mu)$ in minimal supergravity,” *Phys. Rev. Lett.* **87** (2001) 251804, [arXiv:hep-ph/0108037 \[hep-ph\]](#).
- [11] C. Bobeth, T. Ewerth, F. Kruger, and J. Urban, “Enhancement of $B(\text{anti-}B(d) \rightarrow \mu^+\mu^-) / B(\text{anti-}B(s) \rightarrow \mu^+\mu^-)$ in the MSSM with minimal flavor violation and large $\tan\beta$,” *Phys. Rev.* **D66** (2002) 074021, [arXiv:hep-ph/0204225 \[hep-ph\]](#).
- [12] S. Baek, P. Ko, and W. Y. Song, “Implications on SUSY breaking mediation mechanisms from observing $B_s \rightarrow \mu^+\mu^-$ and the muon $(g-2)$,” *Phys. Rev. Lett.* **89** (2002) 271801, [arXiv:hep-ph/0205259 \[hep-ph\]](#).
- [13] A. Dedes, H. K. Dreiner, U. Nierste, and P. Richardson, “Trilepton events and $B_s \rightarrow \mu^+\mu^-$: No lose for mSUGRA at the Tevatron?,” [arXiv:hep-ph/0207026 \[hep-ph\]](#).
- [14] J. K. Mizukoshi, X. Tata, and Y. Wang, “Higgs mediated leptonic decays of B_s and B_d mesons as probes of supersymmetry,” *Phys. Rev.* **D66** (2002) 115003, [arXiv:hep-ph/0208078 \[hep-ph\]](#).
- [15] S. Baek, P. Ko, and W. Y. Song, “SUSY breaking mediation mechanisms and $(g-2) (\mu)$, $B \rightarrow X_s\gamma$, $B \rightarrow X_s\ell^+\ell^-$ and $B_s \rightarrow \mu^+\mu^-$,” *JHEP* **03** (2003) 054, [arXiv:hep-ph/0208112 \[hep-ph\]](#).
- [16] G. Ecker and A. Pich, “The Longitudinal muon polarization in $K_L \rightarrow \mu^+\mu^-$,” *Nucl. Phys.* **B366** (1991) 189–205.
- [17] G. Isidori and R. Unterdorfer, “On the short distance constraints from $K_{L,S} \rightarrow \mu^+\mu^-$,” *JHEP* **01** (2004) 009, [arXiv:hep-ph/0311084 \[hep-ph\]](#).
- [18] G. D’Ambrosio and T. Kitahara, “Direct CP Violation in $K \rightarrow \mu^+\mu^-$,” *Phys. Rev. Lett.* **119** no. 20, (2017) 201802, [arXiv:1707.06999 \[hep-ph\]](#).
- [19] R. Aaij *et al.*, “Improved limit on the branching fraction of the rare decay $K_S^0 \rightarrow \mu^+\mu^-$,” *The European Physical Journal C* **77** no. 10, (Oct, 2017) 678.
- [20] D. Martinez Santos. <https://cds.cern.ch/record/2270191/files/fpcp2017-MartinezSantos.pdf>. LHCb-TALK-2017-164, at FPCP 2017.
- [21] L. Hall, V. Kostelecky, and S. Raby, “New flavor violations in supergravity models,” *Nuclear Physics B* **267** no. 2, (1986) 415 – 432.

- [22] W. Altmannshofer, A. J. Buras, S. Gori, P. Paradisi, and D. M. Straub, “Anatomy and Phenomenology of FCNC and CPV Effects in SUSY Theories,” *Nucl. Phys.* **B830** (2010) 17–94, [arXiv:0909.1333 \[hep-ph\]](#).
- [23] J. Rosiek, “Complete set of Feynman rules for the MSSM: Erratum,” [arXiv:hep-ph/9511250 \[hep-ph\]](#).
- [24] B. C. Allanach *et al.*, “SUSY Les Houches Accord 2,” *Comput. Phys. Commun.* **180** (2009) 8–25, [arXiv:0801.0045 \[hep-ph\]](#).
- [25] A. Crivellin, G. D’Ambrosio, T. Kitahara, and U. Nierste, “ $K \rightarrow \pi\nu\bar{\nu}$ in the MSSM in light of the ϵ'_K/ϵ_K anomaly,” *Phys. Rev.* **D96** no. 1, (2017) 015023, [arXiv:1703.05786 \[hep-ph\]](#).
- [26] T. Blum *et al.*, “The $K \rightarrow (\pi\pi)_{I=2}$ Decay Amplitude from Lattice QCD,” *Phys. Rev. Lett.* **108** (2012) 141601, [arXiv:1111.1699 \[hep-lat\]](#).
- [27] T. Blum *et al.*, “Lattice determination of the $K \rightarrow (\pi\pi)_{I=2}$ Decay Amplitude A_2 ,” *Phys. Rev.* **D86** (2012) 074513, [arXiv:1206.5142 \[hep-lat\]](#).
- [28] T. Blum *et al.*, “ $K \rightarrow \pi\pi$ $\Delta I = 3/2$ decay amplitude in the continuum limit,” *Phys. Rev.* **D91** no. 7, (2015) 074502, [arXiv:1502.00263 \[hep-lat\]](#).
- [29] **RBC, UKQCD** Collaboration, Z. Bai *et al.*, “Standard Model Prediction for Direct CP Violation in $K \rightarrow \pi\pi$ Decay,” *Phys. Rev. Lett.* **115** no. 21, (2015) 212001, [arXiv:1505.07863 \[hep-lat\]](#).
- [30] E. Pallante, A. Pich, and I. Scimemi, “The Standard model prediction for ϵ'_K/ϵ_K ,” *Nucl. Phys.* **B617** (2001) 441–474, [arXiv:hep-ph/0105011 \[hep-ph\]](#).
- [31] T. Hambye, S. Peris, and E. de Rafael, “ $\Delta I = 1/2$ and ϵ'_K/ϵ_K in large N_c QCD,” *JHEP* **05** (2003) 027, [arXiv:hep-ph/0305104 \[hep-ph\]](#).
- [32] H. G. Mullor, “Updated standard model prediction for the kaon direct CP -violating ratio ϵ'_k/ϵ_k ,” 10, 2017. <https://indico.ific.uv.es/indico/contributionDisplay.py?contribId=146&sessionId=6&confId=2960>. Talk given at IX CPAN DAYS.
- [33] G. D’Ambrosio, G. Ecker, G. Isidori, and H. Neufeld, “Radiative non-leptonic kaon decays,” in *2nd DAPHNE Physics Handbook:265-313*, pp. 265–313. 1994. [arXiv:hep-ph/9411439 \[hep-ph\]](#). <http://preprints.cern.ch/cgi-bin/setlink?base=preprint&categ=cern&id=th-7503-94>.
- [34] **Particle Data Group** Collaboration, C. Patrignani *et al.*, “Review of Particle Physics,” *Chin. Phys.* **C40** no. 10, (2016) 100001.
- [35] **SWME** Collaboration, Y.-C. Jang, W. Lee, S. Lee, and J. Leem, “Update on ϵ_K with lattice QCD inputs,” in *35th International Symposium on Lattice Field Theory (Lattice 2017) Granada, Spain, June 18-24, 2017*. 2017. [arXiv:1710.06614 \[hep-lat\]](#).
- [36] M. Endo, T. Goto, T. Kitahara, S. Mishima, D. Ueda, and K. Yamamoto. in preparation.
- [37] T. Kitahara, U. Nierste, and P. Tremper, “Singularity-free next-to-leading order $\Delta S = 1$ renormalization group evolution and ϵ'_K/ϵ_K in the Standard Model and beyond,” *JHEP* **12** (2016) 078, [arXiv:1607.06727 \[hep-ph\]](#).
- [38] S. Descotes-Genon, L. Hofer, J. Matias, and J. Virto, “Global analysis of $b \rightarrow s\ell\ell$ anomalies,” *Journal of High Energy Physics* **2016** no. 6, (Jun, 2016) 92.
- [39] **ATLAS** Collaboration, M. Aaboud *et al.*, “Search for additional heavy neutral Higgs and

gauge bosons in the ditau final state produced in 36 fb^{-1} of pp collisions at $\sqrt{s} = 13 \text{ TeV}$ with the ATLAS detector,” [arXiv:1709.07242 \[hep-ex\]](#).

- [40] A. J. Buras, G. Colangelo, G. Isidori, A. Romanino, and L. Silvestrini, “Connections between ϵ'_K/ϵ_K and rare kaon decays in supersymmetry,” *Nucl. Phys.* **B566** (2000) 3–32, [arXiv:hep-ph/9908371 \[hep-ph\]](#).
- [41] R. Barbieri, R. Contino, and A. Strumia, “ ϵ'_K from supersymmetry with nonuniversal A terms?,” *Nucl. Phys.* **B578** (2000) 153–162, [arXiv:hep-ph/9908255 \[hep-ph\]](#).
- [42] F. Mescia, C. Smith, and S. Trine, “ $K_L \rightarrow \pi^0 e^+ e^-$ and $K_L \rightarrow \pi^0 \mu^+ \mu^-$: A Binary star on the stage of flavor physics,” *JHEP* **08** (2006) 088, [arXiv:hep-ph/0606081 \[hep-ph\]](#).
- [43] W. Altmannshofer, P. Paradisi, and D. M. Straub, “Model-Independent Constraints on New Physics in $b \rightarrow s$ Transitions,” *JHEP* **04** (2012) 008, [arXiv:1111.1257 \[hep-ph\]](#).
- [44] A. J. Buras, R. Fleischer, J. Girrbach, and R. Knegjens, “Probing New Physics with the $B_s \rightarrow \mu^+ \mu^-$ Time-Dependent Rate,” *JHEP* **07** (2013) 77, [arXiv:1303.3820 \[hep-ph\]](#).
- [45] A. Crivellin, J. Heeck, and D. Mueller, “Large $h \rightarrow bs$ in generic two-Higgs-doublet models,” [arXiv:1710.04663 \[hep-ph\]](#).
- [46] A. Pich and E. de Rafael, “Weak K amplitudes in the chiral and $1/N_c$ expansions,” *Phys. Lett.* **B374** (1996) 186–192, [arXiv:hep-ph/9511465 \[hep-ph\]](#).
- [47] J.-M. Gerard, C. Smith, and S. Trine, “Radiative kaon decays and the penguin contribution to the $\Delta I = 1/2$ rule,” *Nucl. Phys.* **B730** (2005) 1–36, [arXiv:hep-ph/0508189 \[hep-ph\]](#).
- [48] M. Gorbahn and U. Haisch, “Charm Quark Contribution to $K_L \rightarrow \mu^+ \mu^-$ at Next-to-Next-to-Leading,” *Phys. Rev. Lett.* **97** (2006) 122002, [arXiv:hep-ph/0605203 \[hep-ph\]](#).
- [49] G. Colangelo, R. Stucki, and L. C. Tunstall, “Dispersive treatment of $K_S \rightarrow \gamma\gamma$ and $K_S \rightarrow \gamma\ell^+\ell^-$,” *Eur. Phys. J.* **C76** no. 11, (2016) 604, [arXiv:1609.03574 \[hep-ph\]](#).
- [50] G. Colangelo and G. Isidori, “Supersymmetric contributions to rare kaon decays: Beyond the single mass insertion approximation,” *JHEP* **09** (1998) 009, [arXiv:hep-ph/9808487 \[hep-ph\]](#).
- [51] M. Endo, S. Mishima, D. Ueda, and K. Yamamoto, “Chargino contributions in light of recent ϵ'_K/ϵ_K ,” *Phys. Lett.* **B762** (2016) 493–497, [arXiv:1608.01444 \[hep-ph\]](#).
- [52] A. J. Buras, M. Gorbahn, S. Jäger, and M. Jamin, “Improved anatomy of ϵ'_K/ϵ_K in the Standard Model,” *JHEP* **11** (2015) 202, [arXiv:1507.06345 \[hep-ph\]](#).
- [53] A. J. Buras and J.-M. Gérard, “Upper bounds on ϵ'_K/ϵ_K parameters $B_6^{(1/2)}$ and $B_8^{(3/2)}$ from large N QCD and other news,” *JHEP* **12** (2015) 008, [arXiv:1507.06326 \[hep-ph\]](#).
- [54] A. J. Buras and J.-M. Gerard, “Final state interactions in $K \rightarrow \pi\pi$ decays: $\Delta I = 1/2$ rule vs. ϵ'_K/ϵ_K ,” *Eur. Phys. J.* **C77** no. 1, (2017) 10, [arXiv:1603.05686 \[hep-ph\]](#).
- [55] L. Lellouch and M. Luscher, “Weak transition matrix elements from finite volume correlation functions,” *Commun. Math. Phys.* **219** (2001) 31–44, [arXiv:hep-lat/0003023 \[hep-lat\]](#).
- [56] G. Colangelo, J. Gasser, and H. Leutwyler, “ $\pi\pi$ scattering,” *Nucl. Phys.* **B603** (2001) 125–179, [arXiv:hep-ph/0103088 \[hep-ph\]](#).
- [57] R. Garcia-Martin, R. Kaminski, J. R. Pelaez, J. Ruiz de Elvira, and F. J. Yndurain, “The Pion-pion scattering amplitude. IV: Improved analysis with once subtracted Roy-like equations up to 1100 MeV,” *Phys. Rev.* **D83** (2011) 074004, [arXiv:1102.2183 \[hep-ph\]](#).

- [58] G. Colangelo. Talk given at the NA62 Physics Handbook MITP Workshop.
- [59] T. Kitahara, U. Nierste, and P. Tremper, “Supersymmetric Explanation of CP Violation in $K \rightarrow \pi\pi$ Decays,” *Phys. Rev. Lett.* **117** no. 9, (2016) 091802, [arXiv:1604.07400 \[hep-ph\]](#).
- [60] A. L. Kagan and M. Neubert, “Large $\Delta I = 3/2$ contribution to ϵ'_K/ϵ in supersymmetry,” *Phys. Rev. Lett.* **83** (1999) 4929–4932, [arXiv:hep-ph/9908404 \[hep-ph\]](#).
- [61] V. Cirigliano, A. Pich, G. Ecker, and H. Neufeld, “Isospin violation in ϵ'_K ,” *Phys. Rev. Lett.* **91** (2003) 162001, [arXiv:hep-ph/0307030 \[hep-ph\]](#).
- [62] V. Cirigliano, G. Ecker, H. Neufeld, and A. Pich, “Isospin breaking in $K \rightarrow \pi\pi$ decays,” *Eur. Phys. J.* **C33** (2004) 369–396, [arXiv:hep-ph/0310351 \[hep-ph\]](#).
- [63] **SWME** Collaboration, J. A. Bailey, Y.-C. Jang, W. Lee, and S. Park, “Standard Model evaluation of ϵ_K using lattice QCD inputs for \hat{B}_K and V_{cb} ,” *Phys. Rev.* **D92** no. 3, (2015) 034510, [arXiv:1503.05388 \[hep-lat\]](#).
- [64] Y. Amhis *et al.*, “Averages of b -hadron, c -hadron, and τ -lepton properties as of summer 2016,” [arXiv:1612.07233 \[hep-ex\]](#).
- [65] D. Bigi, P. Gambino, and S. Schacht, “A fresh look at the determination of $|V_{cb}|$ from $B \rightarrow D^*\ell\nu$,” *Phys. Lett.* **B769** (2017) 441–445, [arXiv:1703.06124 \[hep-ph\]](#).
- [66] B. Grinstein and A. Kobach, “Model-Independent Extraction of $|V_{cb}|$ from $\bar{B} \rightarrow D^*\ell\bar{\nu}$,” *Phys. Lett.* **B771** (2017) 359–364, [arXiv:1703.08170 \[hep-ph\]](#).
- [67] F. U. Bernlochner, Z. Ligeti, M. Papucci, and D. J. Robinson, “Tensions and correlations in $|V_{cb}|$ determinations,” *Phys. Rev.* **D96** no. 9, (2017) 091503, [arXiv:1708.07134 \[hep-ph\]](#).
- [68] A. Bevan *et al.*, “Standard Model updates and new physics analysis with the Unitarity Triangle fit,” *Nucl. Phys. Proc. Suppl.* **241-242** (2013) 89–94.
- [69] **KLOE** Collaboration, F. Ambrosino *et al.*, “Determination of CP and CPT violation parameters in the neutral kaon system using the Bell-Steinberger relation and data from the KLOE experiment,” *JHEP* **12** (2006) 011, [arXiv:hep-ex/0610034 \[hep-ex\]](#).
- [70] A. Crivellin and M. Davidkov, “Do squarks have to be degenerate? Constraining the mass splitting with Kaon and D mixing,” *Phys. Rev.* **D81** (2010) 095004, [arXiv:1002.2653 \[hep-ph\]](#).
- [71] F. Gabbiani, E. Gabrielli, A. Masiero, and L. Silvestrini, “A Complete analysis of FCNC and CP constraints in general SUSY extensions of the standard model,” *Nucl. Phys.* **B477** (1996) 321–352, [arXiv:hep-ph/9604387 \[hep-ph\]](#).
- [72] A. J. Buras, D. Guadagnoli, and G. Isidori, “On ϵ_K Beyond Lowest Order in the Operator Product Expansion,” *Phys. Lett.* **B688** (2010) 309–313, [arXiv:1002.3612 \[hep-ph\]](#).
- [73] **RBC/UKQCD** Collaboration, N. Garron, R. J. Hudspith, and A. T. Lytle, “Neutral Kaon Mixing Beyond the Standard Model with $n_f = 2 + 1$ Chiral Fermions Part 1: Bare Matrix Elements and Physical Results,” *JHEP* **11** (2016) 001, [arXiv:1609.03334 \[hep-lat\]](#).
- [74] J. A. Bagger, K. T. Matchev, and R.-J. Zhang, “QCD corrections to flavor changing neutral currents in the supersymmetric standard model,” *Phys. Lett.* **B412** (1997) 77–85, [arXiv:hep-ph/9707225 \[hep-ph\]](#).
- [75] D. M. Santos, P. Álvarez Cartelle, M. Borsato, V. G. Chobanova, J. G. Pardinñas, M. L. Martínez, and M. R. Pernas, “Ipanema- β : tools and examples for hep analysis on gpu,” [arXiv:1706.01420 \[hep-ex\]](#).

- [76] J. Brest, S. Greiner, B. Boskovic, M. Mernik, and V. Zumer, “Self-Adapting Control Parameters in Differential Evolution: A Comparative Study on Numerical Benchmark Problems,” *IEEE Transactions on Evolutionary Computation* **10** (2006) 646–657.
- [77] P. A. R. Ade *et al.*, “Planck 2015 results xiii. cosmological parameters,” *Astronomy & Astrophysics* **594** no. A13, (Oct, 2016) .
- [78] J. C. Costa *et al.*, “Likelihood Analysis of the Sub-GUT MSSM in Light of LHC 13-TeV Data,” [arXiv:1711.00458 \[hep-ph\]](#).
- [79] E. Bagnaschi *et al.*, “Likelihood Analysis of the pMSSM11 in Light of LHC 13-TeV Data,” [arXiv:1710.11091 \[hep-ph\]](#).
- [80] E. A. Bagnaschi *et al.*, “Supersymmetric Dark Matter after LHC Run 1,” *Eur. Phys. J.* **C75** (2015) 500, [arXiv:1508.01173 \[hep-ph\]](#).
- [81] E. Bagnaschi *et al.*, “Likelihood Analysis of the Minimal AMSB Model,” *Eur. Phys. J.* **C77** no. 4, (2017) 268, [arXiv:1612.05210 \[hep-ph\]](#).
- [82] A. Cuoco, J. Heisig, M. Korsmeier, and M. Krämer, “Constraining heavy dark matter with cosmic-ray antiprotons,” [arXiv:1711.05274 \[hep-ph\]](#).
- [83] J. Hisano, S. Matsumoto, M. Nagai, O. Saito, and M. Senami, “Non-perturbative effect on thermal relic abundance of dark matter,” *Phys. Lett.* **B646** (2007) 34–38, [arXiv:hep-ph/0610249 \[hep-ph\]](#).
- [84] M. Ibe, S. Matsumoto, and R. Sato, “Mass Splitting between Charged and Neutral Winos at Two-Loop Level,” *Phys. Lett.* **B721** (2013) 252–260, [arXiv:1212.5989 \[hep-ph\]](#).
- [85] R. Harnik, D. T. Larson, H. Murayama, and A. Pierce, “Atmospheric neutrinos can make beauty strange,” *Phys. Rev.* **D69** (2004) 094024, [arXiv:hep-ph/0212180 \[hep-ph\]](#).